bioRxiv preprint doi: https://doi.org/10.64898/2026.10.23.761465; this version posted October 31, 2026. The copyright holder for this preprint (which was not certified by peer review) is the author/funder, who has granted bioRxiv a license to display the preprint in perpetuity. It is made available under a CC-BY-NC-ND 4.0 International license.

Siderophore-Mediated Competition Between Cystic Fibrosis Pathogens Increases Virulence Factor Production

Niladri Bhowmik[1], Laura Rodriguez-Velandia[2], Mercedes Pérez Pérez[1], Sydney M. Morabbi[1], Laura M. Sanchez[2], and Reed M. Stubbendieck[1,#]

[1]Department of Microbiology and Molecular Genetics, Oklahoma State University, Stillwater, OK 74078

[2]Department of Chemistry and Biochemistry, University of California, Santa Cruz, Santa Cruz, CA 95064

Running Title: Competition for Iron Between CF Pathogens Increases Virulence

Keywords: *Achromobacter*, alcaligin, bacterial competition, cystic fibrosis, iron, *Pseudomonas aeruginosa*, pyoverdine, secondary metabolite, siderophore, virulence

[#]Address correspondence to Reed M. Stubbendieck (stubbendieck@okstate.edu)

bioRxiv preprint doi: https://doi.org/10.64898/2026.10.23.761465; this version posted October 31, 2026. The copyright holder for this preprint (which was not certified by peer review) is the author/funder, who has granted bioRxiv a license to display the preprint in perpetuity. It is made available under a CC-BY-NC-ND 4.0 International license.

Abstract

The airways of people with cystic fibrosis (CF) are colonized by a polymicrobial community and coinfections with multiple pathogens may exacerbate disease. By analyzing 16S rRNA gene sequencing datasets, we determined that *Achromobacter-Pseudomonas* coinfection was associated with worse lung function than infection with either pathogen alone, or coinfections with *Pseudomonas* and other CF bacterial pathogens. We discovered *Achromobacter* spp. induced production of the siderophore pyoverdine by *Pseudomonas aeruginosa* strain PAO1 and other clinical isolates on synthetic CF sputum medium (SCFM), supplemented with physiologically relevant iron concentrations. We then tested 21 *Achromobacter* strains, encompassing seven species, and determined that 17 (81%) induced pyoverdine production. We sequenced the full genomes of these *Achromobacter* and found 18 (86%) encoded a biosynthetic gene cluster for the production of alcaligin. This compound is an iron-chelating siderophore that has previously been shown to be involved in colonization of the respiratory tract by *Bordetella* spp. Using mass spectrometry imaging, we confirmed that *Achromobacter dolens* strain RMS0405 produces alcaligin during coculture with PAO1. Further, we found that supplementing SCFM with increasing iron abolishes pyoverdine induction by PAO1 during coculture. Pyoverdine is known to contribute directly to virulence and regulate expression of other virulence factors. Using transcriptomics and proteomics, we determined that RMS0405 induces a low-iron stress response in PAO1 and stimulates the production of exotoxin A and other known virulence factors. Together, our results indicate that *Achromobacter* spp. and *P. aeruginosa* may exacerbate virulence in the airways of people with CF as a byproduct of competition for iron.

bioRxiv preprint doi: https://doi.org/10.64898/2026.10.23.761465; this version posted October 31, 2026. The copyright holder for this preprint (which was not certified by peer review) is the author/funder, who has granted bioRxiv a license to display the preprint in perpetuity. It is made available under a CC-BY-NC-ND 4.0 International license.

Importance

Within polymicrobial infections, competition between pathogens is thought to attenuate virulence, as microbes direct resources away from pathogenesis and toward microbial interactions. However, by coculturing the cystic fibrosis pathogens *Achromobacter* spp. and *Pseudomonas aeruginosa*, we determined that competition induces pyoverdine production by the latter pathogen. This secondary metabolite functions in iron acquisition, is cytotoxic toward eukaryotic cells, and activates production of other virulence factors. We demonstrated that production of the siderophore alcaligin by *Achromobacter dolens* imposes iron limitation and induces pyoverdine production by *P. aeruginosa*. Our finding challenges a conventional view that competition limits pathogenic potential, and instead suggests that interactions between coinfecting microbes can amplify virulence. Notably, disrupting the signals or pathways that drive competitive upregulation of virulence factors could attenuate disease severity without relying on traditional antibiotics. This approach could open new avenues for understanding pathogenesis and for developing virulence factor-targeting therapeutics tailored to polymicrobial infections.

bioRxiv preprint doi: https://doi.org/10.64898/2026.10.23.761465; this version posted October 31, 2026. The copyright holder for this preprint (which was not certified by peer review) is the author/funder, who has granted bioRxiv a license to display the preprint in perpetuity. It is made available under a CC-BY-NC-ND 4.0 International license.

Introduction

Cystic fibrosis (CF) is a multisystem disease caused by mutations in the gene encoding the CF transmembrane conductance regulator (*CFTR*). These mutations disrupt chloride ion transport activity, resulting in the accumulation of a thick and adherent mucus that provides a niche for microbial colonization (1, 2). Impaired mucociliary clearance promotes chronic infection, during which pathogens in the airways of people with CF (pwCF) produce virulence factors that damage epithelial tissues, leading to lung function decline, and, ultimately, death. Despite recent advancements in treatment, including development of CFTR modulators, such as elexacaftor/tezacaftor/ivacaftor (ETI), CF remains a life-shortening disease with significant morbidity and mortality, reflected in a median age of death of 37 years (3).

The most well-characterized pathogen in the airways of pwCF is *Pseudomonas aeruginosa*. Advances in metagenomics and culturomics revealed that the airways of pwCF are colonized by a complex microbiota that includes other oropharyngeal and pathogenic bacteria (4–6). We recently showed that these two groups of bacteria colonize the CF airway with distinct patterns. Oropharyngeal genera are prevalent but rarely abundant, whereas pathogens are less prevalent but often reach high relative abundance when present. These microbiota states are associated with different clinical outcomes for pwCF (7). Our data further suggested that pathogens come to dominate in part by producing bioactive metabolites to inhibit other members of the CF airway microbiota (7). Among CF pathogens, the roles that bioactive metabolites play in interactions between *P. aeruginosa* and *Staphylococcus aureus* have been well established (8–11). However, the consequences of these metabolite-mediated interactions between *P. aeruginosa* and other CF pathogens, and their impact on disease, are less understood.

bioRxiv preprint doi: https://doi.org/10.64898/2026.10.23.761465; this version posted October 31, 2026. The copyright holder for this preprint (which was not certified by peer review) is the author/funder, who has granted bioRxiv a license to display the preprint in perpetuity. It is made available under a CC-BY-NC-ND 4.0 International license.

Achromobacter spp. are Gram-negative bacteria commonly found within both terrestrial and aquatic environments. These bacteria have emerged as pathogens in the airways of pwCF over the last 30 years, rising globally in incidence from approximately 2-3% in the 1990s to approximately 7-10% in the early 2020s (12). The type species is *Achromobacter xylosoxidans*, however early studies did not distinguish between this and ten other *Achromobacter* spp. that are now known to infect the airways of pwCF (13–15). Infections with *Achromobacter* are associated with a strong inflammatory response due to the production of siderophores, type III secretion, and type VI secretion systems (16–23). *Achromobacter* infections are associated with severe loss-of-function *CFTR* genotypes, including those that do not respond to ETI, and are difficult to treat due to the multidrug resistance of these pathogens. Thus, infection with *Achromobacter* remains a threat to pwCF with the fewest therapeutic options (23–26).

Approximately half of pwCF with chronic *Achromobacter* infection are coinfected with *P. aeruginosa.* These coinfections are frequently associated with more severe clinical outcomes and greater annual decrease in pulmonary health (16–19, 23, 27). Few studies have directly characterized interactions between *Achromobacter* spp. and *P. aeruginosa*. For instance, Menetrey et al. tested 53 *A. xylosoxidans-P. aeruginosa* pairs in coculture assays, finding eleven instances of growth inhibition, two instances of motility reduction, and seven instances of pigment reduction in *P. aeruginosa* (28). Besse and Menetrey et al. further showed that *A. xylosoxidans* strain Ax 200 altered the *P. aeruginosa* proteome, reducing production of proteins involved in swimming, biofilm formation, and siderophore production. Accordingly, the mortality of *Danio rerio* embryos coinfected with *A. xylosoxidans* Ax 200 and *P. aeruginosa* was halved, compared to infection with *P. aeruginosa* alone (29). Similarly, Sahl et al. recently reported that early-infection CF isolates of *A. xylosoxidans* inhibit *P. aeruginosa* biofilm

bioRxiv preprint doi: https://doi.org/10.64898/2026.10.23.761465; this version posted October 31, 2026. The copyright holder for this preprint (which was not certified by peer review) is the author/funder, who has granted bioRxiv a license to display the preprint in perpetuity. It is made available under a CC-BY-NC-ND 4.0 International license.

formation *in vitro* (30). Although the mechanisms underlying virulence attenuation and biofilm inhibition remain unclear, Soh et al. previously demonstrated that 12 of 17 CF-associated *A. xylosoxidans* strains they tested inactivated the *Pseudomonas* quinolone signal (31), which is necessary for these virulence phenotypes (32). In addition to antagonism, Menetrey et al. also identified nine instances of growth promotion, eight instances of motility increase, and one instance of increased pigment production by *P. aeruginosa* during coculture with *A. xylosoxidans* (28). Thus, *Achromobacter* spp. can alter virulence-associated phenotypes in *P. aeruginosa* positively and negatively, but the specific mechanisms underlying these interactions are not well-understood.

In this study, we show that *Achromobacter-Pseudomonas* coinfection is associated with more severe disease than infection with either pathogen alone. During coculture, *Achromobacter* spp. impose iron limitation that induces production of pyoverdine, activates an iron-starvation response, and increases production of extracellular virulence factors by *P. aeruginosa*. Together, these data suggest that CF pathogens engage in exploitation competition for iron in the airways, which may lead to collateral damage to the host.

bioRxiv preprint doi: https://doi.org/10.64898/2026.10.23.761465; this version posted October 31, 2026. The copyright holder for this preprint (which was not certified by peer review) is the author/funder, who has granted bioRxiv a license to display the preprint in perpetuity. It is made available under a CC-BY-NC-ND 4.0 International license.

Results

Coinfections with *Achromobacter* and *Pseudomonas* exacerbate lung function outcomes in pwCF. We wanted to assess the impact of coinfection with *Achromobacter* and *Pseudomonas* on lung function through a reanalysis of 16S rRNA gene amplicon sequencing studies (7) (**Table S1** in the supplemental material). We limited our analyses to the genus level, because the 16S rRNA gene possesses variable and low resolution below this taxonomic level (33, 34).

To evaluate lung function, we used the forced expiratory volume in 1 s percent predicted (FEV_1 pp) metric. We grouped samples based on whether they contained no pathogens (n=49), *Achromobacter* alone (n=43), *Pseudomonas* alone (n=709), or both pathogens together (n=58), using a 1% relative abundance threshold. There were significant differences in lung function across the groups (Kruskal-Wallis $\chi^2 = 16.3$, df = 3, $P < 0.001$). Relative to when no pathogen was detected, pwCF with either *Achromobacter* or *Pseudomonas* alone had FEV_1 pp values about 9 to 10 points lower, whereas those with both pathogens had values lower by about 20 points (**Fig. 1A**). Across relative abundance thresholds ranging from 0.1% to 5%, this relationship held (**Fig. S1A** in the supplemental material). We found that higher combined abundance of the two pathogens was associated with lower FEV_1 pp values. Further, pwCF whose airway microbiota was dominated (combined relative abundance >50%) by *Achromobacter* and *Pseudomonas* had the lowest FEV_1 pp values (median 42.0 FEV_1 pp, interquartile range [IQR]: 27 to 52 FEV_1 pp), compared to those in which the two pathogens made up a smaller fraction (<50% relative abundance) of the microbiota (median: 68.5 FEV_1 pp, IQR: 45 to 86 FEV_1 pp) (Wilcoxon rank-sum test P = 0.018) (see **Fig. S1B** in the supplemental material).

bioRxiv preprint doi: https://doi.org/10.64898/2026.10.23.761465; this version posted October 31, 2026. The copyright holder for this preprint (which was not certified by peer review) is the author/funder, who has granted bioRxiv a license to display the preprint in perpetuity. It is made available under a CC-BY-NC-ND 4.0 International license.

The proportion of pwCF with severe disease differed between the four groups (χ^2 = 19.3, df = 3, *P* < 0.001). Specifically, we found that pwCF coinfected with both pathogens were three to fourfold more likely to have severe lung disease (defined as FEV_1 pp ≤ 30%) than those with *Achromobacter* or *Pseudomonas* alone (**Fig. 1B**). This effect was specific to *Achromobacter*, as coinfection with *Burkholderia*, *Haemophilus*, *Staphylococcus*, or *Stenotrophomonas* did not significantly alter lung function, relative to *Pseudomonas* alone (**Fig. 1C**). Thus, these data support clinical studies concluding that coinfection with *Achromobacter* spp. and *P. aeruginosa* lead to worse patient outcomes.

Pyoverdine production is induced by *P. aeruginosa* when cocultured with *Achromobacter* spp. During a previous screen of 1,597 bacterial isolates from pwCF for inhibitory activity (7), we observed that *Achromobacter* isolates increased production of a green pigment by *P. aeruginosa*. We repeated these coculture assays on synthetic cystic fibrosis sputum medium (SCFM) supplemented with 25 μM ferric chloride ($FeCl_3$) to mimic physiological concentrations of ferric iron (Fe^{3+}) in the airways of pwCF (35, 36). We allowed the *Achromobacter* isolate to establish for 72 h after which we inoculate the *P. aeruginosa* perpendicularly to the established culture. After overnight coincubation, we confirmed that *Achromobacter dolens* strain RMS0405 induced production of a green pigment in *P. aeruginosa* strain PAO1 (**Fig. 2A**). We suspected that coculture with *A. dolens* induced pyoverdine, because we observed fluorescence when placing plates in a blue light (~470 nm) transilluminator (**Fig. 2B**). We repeated cocultures with *A. dolens* using a Δ*pvdA* mutant that is unable to produce pyoverdine and confirmed loss of pigment production which was restored upon complementation with *pvdA* (Δ*pvdA* + *pvdA*) (**Fig. 2AB**). We observed no production of pyoverdine from *P. aeruginosa* in monoculture under these conditions (**Fig. 2C**). Together, these data indicate that *A. dolens* induces production of pyoverdine by *P. aeruginosa* during coculture.

bioRxiv preprint doi: https://doi.org/10.64898/2026.10.23.761465; this version posted October 31, 2026. The copyright holder for this preprint (which was not certified by peer review) is the author/funder, who has granted bioRxiv a license to display the preprint in perpetuity. It is made available under a CC-BY-NC-ND 4.0 International license.

A. dolens induces pyoverdine production in clinical _Pseudomonas_ isolates. Our assays were performed using *P. aeruginosa* strain PAO1, a laboratory strain that was originally isolated from an infected wound (37). To determine if pyoverdine induction extended beyond PAO1, we tested *A. dolens* strain RMS0405 against 48 clinical isolates of *Pseudomonas* from different pwCF that previously isolated (7) (**Table S2** in the supplemental material). Because most isolates were identified only by sequencing the 16S rRNA V3–V4 region, we refer to them as *Pseudomonas*. As a control, we also inoculated each of these *Pseudomonas* isolates on SCFM with no added iron (SCFM + 0 μM $FeCl_3$) without *A. dolens*, to assess whether they would produce pyoverdine under iron-limiting conditions.

Twenty (41.7%) isolates did not produce pyoverdine in monoculture or when cocultured. Accordingly, when we screened these isolates for *pvdA* using PCR, we found 5 (25%) did not yield a PCR product. We presume that the other 15 isolates possess mutations that abrogate pyoverdine biosynthesis. Two isolates (4.2%) produced pyoverdine in response to *A. dolens*, but not in response to iron limitation. However, eight (16.7%) isolates only produced pyoverdine in response to iron limitation. Finally, eighteen (37.5%) isolates produced pyoverdine in response to iron limitation and *A. dolens*. Together, 18 of 26 (69.2%) *pvdA*-positive *Pseudomonas* isolates produced pyoverdine under iron-limiting conditions and during coculture, suggesting that the response to *A. dolens* is common, but not ubiquitous, in *Pseudomonas* (**Table 1**).

Multiple species of _Achromobacter_ induce pyoverdine production in _P. aeruginosa_. We tested twenty additional strains of *Achromobacter* spp., encompassing seven of the eleven species previously reported in the airways of pwCF (12), isolated from multiple sources and tested their ability to induce pyoverdine production in *P. aeruginosa* strain PAO1, as above. In total, we found that 17/21 (81.0%) of *Achromobacter* spp. induced production of pyoverdine in *P. aeruginosa*. Each *Achromobacter* species

bioRxiv preprint doi: https://doi.org/10.64898/2026.10.23.761465; this version posted October 31, 2026. The copyright holder for this preprint (which was not certified by peer review) is the author/funder, who has granted bioRxiv a license to display the preprint in perpetuity. It is made available under a CC-BY-NC-ND 4.0 International license.

that we tested was able to induce pyoverdine. However, 4/11 (36.4%) strains of *A. xylosoxidans* did not induce pyoverdine when cocultured with *P. aeruginosa* (**Fig. 3A**). We note here that strains DSM 6388, DSM 26073, and MN001 were deposited as *A. xylosoxidans*, but a core genome phylogeny and average nucleotide identity (ANI) to type species classified them as *Achromobacter insuavis* (99.2% ANI), *A. insuavis* (99.8% ANI), and *Achromobacter ruhlandii* (98.4% ANI), respectively. Together, these data suggest the ability to induce pyoverdine is widespread, but not universal, among *Achromobacter* spp.

***Achromobacter* spp. encode a biosynthetic gene cluster for production of the siderophore alcaligin**. Because pyoverdine is produced under iron limitation, we hypothesized that siderophores produced by *Achromobacter* may induce its production. Previous work demonstrated that siderophore production is widespread among *Achromobacter* isolates and is more common in clinical *Achromobacter* isolates than in environmental isolates (22). Therefore, to characterize siderophore production in *Achromobacter* spp., we performed whole genome sequencing for all *Achromobacter* strains that had not been sequenced, and used antiSMASH and BiG-SCAPE to identify biosynthetic gene clusters (BGCs) and group them into gene cluster families (GCFs).

Each *Achromobacter* spp. encoded a median of 12 BGCs or BGC fragments per genome (IQR: 11 to 13 BGCs or BGC fragments per genome) (**Fig. 3A**). Eighteen (86%) *Achromobacter* spp. strains, encompassing five of seven species that we tested, and all CF strains, encoded a BGC with high sequence similarity to the non-ribosomal independent siderophore (NIS) BGC for alcaligin (*alc*) from *Bordetella pertussis* strain Tohama I (**Fig. 3B** and **Fig. S2** in the supplemental material). Fourteen (82.3%) of *Achromobacter* strains that induced pyoverdine production encoded this BGC. Four strains of *A. xylosoxidans* encoded this BGC but did not induce pyoverdine. In addition, three *Achromobacter* spp. induced pyoverdine production, but did not encode the *alc* BGC (**Fig. 3A**).

bioRxiv preprint doi: https://doi.org/10.64898/2026.10.23.761465; this version posted October 31, 2026. The copyright holder for this preprint (which was not certified by peer review) is the author/funder, who has granted bioRxiv a license to display the preprint in perpetuity. It is made available under a CC-BY-NC-ND 4.0 International license.

Alcaligin (**Fig. 3C**) is a dihydroxamate iron-binding siderophore that is essential for lung colonization by *B. pertussis and Bordetella bronchiseptica* (38, 39). Alcaligin was originally reported from *A. xylosoxidans* strain KN 3-1 (formerly *Alcaligenes denitrificans* subsp. *xylosoxidans*), isolated from lagoon sediment (40, 41), but its production from CF isolates of *Achromobacter* has yet to be confirmed. We confirmed that all *Achromobacter* strains with the *alc* BGC possess all genes necessary for the proposed biosynthesis of alcaligin starting from L-ornithine (**Fig. S3A** in the supplemental material). These strains also encoded genes for the proteins involved in alcaligin regulation (*alcR*) (42–44), export (*alcS*) (45), uptake of ferri-alcaligin (*fauA*) (39, 46), and reductive release of iron (*alcD*) (43). There were weak hits to *alcS* and *fauA* in *alc* negative strains, which may represent other major facilitator superfamily or TonB-dependent transporters. As these strains lack *alcD*, it is unlikely that they would be able to utilize alcaligin (see **Fig. S2** and **Fig. S3B** in the supplemental material).

***A. dolens* produces a siderophore.** An agar extract from *A. dolens* strain RMS0405 cultured on SCFM possessed chrome azurol S activity (**Fig. 3D**), confirming siderophore production by this strain (47).

***A. dolens* produces alcaligin and *P. aeruginosa* produces pyoverdine and pyochelin during coculture.** We next examined siderophore production during coculture of *A. dolens* strain RMS0405 and *P. aeruginosa* strain PAO1 or the Δ*pvdA* mutant. Consistent with our previous results, we detected fluorescence from the wild-type strain (**Fig. 4A**), but not from the Δ*pvdA* mutant (**Fig. 4B**).

We then used matrix-assisted laser desorption/ionization mass spectrometry (MALDI-MSI) to identify and map the distribution of metabolites produced by *A. dolens* and *P. aeruginosa* over the agar surface of the coculture. We identified an ion corresponding to pyoverdine E (*m/z* 1333.6177 ± 4.6 parts

bioRxiv preprint doi: https://doi.org/10.64898/2026.10.23.761465; this version posted October 31, 2026. The copyright holder for this preprint (which was not certified by peer review) is the author/funder, who has granted bioRxiv a license to display the preprint in perpetuity. It is made available under a CC-BY-NC-ND 4.0 International license.

per million [ppm] $[M+H]^+$), the major variant produced by *P. aeruginosa* strain PAO1 (48) from wild type (**Fig. 4C**), but not the Δ*pvdA* mutant (**Fig. 4D**). We then confirmed production of alcaligin (*m/z* 405.1866 $[M+H]^+$) by *A. dolens* in both cocultures (**Fig. 4E-F**). We also identified two ions that likely correspond to alcaligin (*m/z* 405.1907 $[M+H]^+$) and a +2 Da analogue (*m/z* 407.2865 $[M+H]^+$) (**Fig. S4** in the supplemental material**)**. We examined cocultures for production of pyochelin (*m/z* 325.0692 $[M+H]^+$), the second major siderophore of *P. aeruginosa*. Strikingly, we observed that pyochelin was produced more abundantly by the Δ*pvdA* mutant than the wild type (**Fig. 4G-H**). We speculated that *P. aeruginosa* Δ*pvdA* increases production of pyochelin in coculture with *A. dolens* to compensate for loss of pyoverdine production. We generated a pyochelin biosynthesis mutant (Δ*pchA*) and a pyoverdine/pyochelin double biosynthesis mutant (Δ*pvdA* Δ*pchA*) and tested them in coculture with *A. dolens* on SCFM with no supplemented $FeCl_3$. Under these conditions, we observed a minor growth defect of the Δ*pvdA* mutant that was more pronounced in the Δ*pvdA* Δ*pchA* mutant (**Fig. S5** in the supplemental material). We did not observe any other differences in production of known *P. aeruginosa* secondary metabolites between wild type or Δ*pvdA* (**Fig. S6** in the supplemental material).

We performed MALDI-QqTOF data-dependent tandem mass spectrometry (MALDI-TOF-DDA-MS^2) to validate these siderophores. Based on a library match, we confirmed pyoverdine E (*m/z* 1333.6143) by the wild-type *P. aeruginosa* (**Fig. S7A** in the supplemental material). We assigned *m/z* 405.1980 as alcaligin because SIRIUS predicted the formula $C_{16}H_{28}N_4O_8$, consistent with alcaligin (**Fig. S7B** in the supplemental material), although the MALDI-MS/MS spectrum did not match predicted ESI fragmentation patterns in reference databases. This is likely due to difference in ionization sources and the collision energies that arise during ion formation. We have observed this phenomenon in other experiments, and this is an active area of research to determine how different ionization sources impact the resulting MS/MS spectra. Similarly, we assigned *m/z* 325.0675 as pyochelin based on an exact mass

bioRxiv preprint doi: https://doi.org/10.64898/2026.10.23.761465; this version posted October 31, 2026. The copyright holder for this preprint (which was not certified by peer review) is the author/funder, who has granted bioRxiv a license to display the preprint in perpetuity. It is made available under a CC-BY-NC-ND 4.0 International license.

match to the expected formula and high-quality MS/MS data (**Fig. S7C** in the supplemental material). Together, these data indicate that siderophores are produced by both *A. dolens* and *P. aeruginosa* during coculture.

Iron supplementation abolishes pyoverdine induction by *P. aeruginosa* during coculture with *A. dolens*. We hypothesized that competition for Fe^{3+} between *Achromobacter* spp. and *P. aeruginosa* leads to pyoverdine production. To test this hypothesis, we repeated the coculture assays between *A. dolens* strain RMS0405 and *P. aeruginosa* strain PAO1 on SCFM, but varied the concentration of supplemented Fe^{3+} (**Fig. 5**). With no added iron (outside of trace iron in our water and glassware), we observed production of pyoverdine in coculture (**Fig. 5A**) and monoculture (**Fig. 5D**). As before, on SCFM + 25 μM $FeCl_3$, pyoverdine was induced in coculture (**Fig. 5B**), but not monoculture (**Fig. 5E**). Finally, on SCFM + 100 μM $FeCl_3$, pyoverdine was not produced under either condition (**Fig. 5C, F**). For all experiments, there was no production of pyoverdine by the Δ*pvdA* mutant, and the complement behaved like wild type. These results support a model wherein pyoverdine is induced by iron depletion by *Achromobacter* spp. using alcaligin or other siderophores.

Coculture with *A. dolens* activates expression of the low-iron stress response in *P. aeruginosa.* We compared the transcriptomes of *P. aeruginosa* cultured on SCFM + 25 μM $FeCl_3$ in monoculture and in coculture with *A. dolens*. We harvested RNA after 12 h, just before production of pyoverdine is visible under blue light. Coculture with *A. dolens* significantly altered the transcriptional profile of *P. aeruginosa*, resulting in 366 genes with increased expression and 253 genes with decreased expression (**Fig. 6A** and **Table S3** in the supplemental material). We observed that expression of most (14/16) pyoverdine biosynthesis genes (median: +1.5×, IQR: +1.4 to +1.6×, Benjamini-Hochberg [BH]-adjusted P = 3.e-15), and the *fpvA* (+1.3×, BH-adjusted P = 2.4e-2) and *fpvB* (+2.1×, BH-adjusted P = 1.0e-6) genes, which

bioRxiv preprint doi: https://doi.org/10.64898/2026.10.23.761465; this version posted October 31, 2026. The copyright holder for this preprint (which was not certified by peer review) is the author/funder, who has granted bioRxiv a license to display the preprint in perpetuity. It is made available under a CC-BY-NC-ND 4.0 International license.

284 encode for ferripyoverdine importers, were increased during coculture. In addition, we found that
285 expression other outer membrane TonB-dependent receptors (median: +1.3× IQR: +1.0 to +1.8×, BH-
286 adjusted *P* = 2.5e-5), and the hemophore-encoding *hasAp* (49) (+1.6×, BH-adjusted *P* = 3.1e-2) were also
287 increased during coculture.
288
289 We identified a total of 95 promoters in the *P. aeruginosa* strain PAO1 genome that contained
290 putative ferric uptake regulator (Fur) binding site (FBS) sequences (**Fig. 6B** and **Table S4** in the
291 supplemental material). We found that 28 (29.5%) of these genes were upregulated during coculture,
292 compared to 338/5,333 (6.3%) of genes lacking an upstream putative FBS (Fisher's exact OR = 6.2, *P* =
293 8.4e-12) (**Fig. 6C**). 10.4% of genes with increased coculture expression had putative FBS, which was a 9.0-
294 fold increase over monoculture (Fisher's exact odds ratio [OR] = 9.8, *P* = 9.9e-5) (**Fig. 6C inset**).
295
296 There were 10 gene sets with increased (n=7) or decreased (n=3) expression in *P. aeruginosa*
297 during coculture (**Fig. 6D**). These decreased pathways encode proteins that are large iron sinks. For
298 instance, the genes for NADH dehydrogenase I (complex I) and the cytochrome bc_1 complex in the
299 "oxidative phosphorylation" pathway use Fe-S clusters and a Rieske [2Fe-2S] center together with heme,
300 respectively, are decreased. In addition, the genes for *fumC1* (+2.0×, BH-adjusted *P* = 5.7e-3), which
301 encodes an alternative non-Fe-S-containing fumarase and *mqoA* (+2.4×, BH-adjusted *P* = 2.9e-8), which
302 encodes a malate:quinone oxidoreductase that bypasses complex I, are upregulated in during coculture.
303 Within the "formate and one-carbon metabolism pathway", expression of the catalase *katA* (−2.8×, BH-
304 adjusted *P* = 2.5e-8) and formate dehydrogenase *fdnGHI* (−1.5 to −1.7×, BH-adjusted *P* ≤ 1.0e-2) genes,
305 which contain heme and Fe-S clusters, respectively, are decreased. Furthermore, expression of *acnA*
306 (−1.4×, BH-adjusted *P* = 2.1e-3), which encodes aconitase, and *moaA1* (−2.8×, BH-adjusted *P* = 5.8e-4)
307 and *moaA2* (−1.4×, BH-adjusted *P* = 1.3e-2) genes for molybdopterin biosynthesis, which each harbor

bioRxiv preprint doi: https://doi.org/10.64898/2026.10.23.761465; this version posted October 31, 2026. The copyright holder for this preprint (which was not certified by peer review) is the author/funder, who has granted bioRxiv a license to display the preprint in perpetuity. It is made available under a CC-BY-NC-ND 4.0 International license.

two [4Fe-4S] clusters were decreased. Moreover, the *isc* operon for Fe-S cluster assembly was increased (+1.3 to +1.8×, BH-adjusted *P* = 1.3e-12), potentially due lack of a [2Fe-2S] cluster in the regulator IscR. Together, these data suggest that coculture with *A. dolens* stimulates a low-iron stress response in *P. aeruginosa*.

Coculture with *A. dolens* may also shift *P. aeruginosa* to alternative carbon and sulfur sources and alter expression of type VI secretion and phenazine biosynthesis genes. Coculture with *A. dolens* strain RMS0405 significantly altered expression of metabolic pathways in *P. aeruginosa* strain PAO1 (**Fig. 6D**). In coculture, *P. aeruginosa* upregulated expression of the *bkdA1*, *bkdA2*, and *bkdB* (+1.4× to +1.7×, BH-adjusted *P* < 1.0e-3) and *liuABCD* (median: +1.8×, IQR: +1.7 to +1.9×, BH-adjusted *P* = 2.9e-4) genes, which are involved in leucine catabolism. This suggests that *A. dolens* depletes the available glucose and lactate in SCFM before *P. aeruginosa* is cultured. The most highly induced genes during coculture were for acetoin and 2,3-butanediol metabolism (median: +150×, IQR: +120 to +200×, BH-adjusted *P* = 1.2e-7). Accordingly, *A. dolens* encodes a diacetyl reductase that is predicted to produce (*S*)-acetoin as a byproduct of pyruvate metabolism. Furthermore, *A. dolens* may deplete the available sulfur, as all 15 genes for sulfate transport and assimilation and for taurine and alkanesulfonate scavenging were upregulated (median: +2.6×, IQR: +1.9 to +3.4×, BH-adjusted *P* = 2.1e-16) during coculture.

Coculture with *A. dolens* increased expression of the Hcp secretion island I (H1) type VI secretion system (T6SS) genes (median: +1.6×, IQR: +1.3 to +1.7×, BH-adjusted *P* = 1.2e-10) in *P. aeruginosa* (**Fig. 6D**). The T6SS is involved in interspecies bacterial competition and delivers toxic effectors into the periplasm of target cells (50). Expression of the effector genes *tse1* (+1.8×, BH-adjusted *P* = 8.7e-4) and *tse3* (+1.5×, BH-adjusted *P* = 6.4e-4) increased in coculture. Coculture also affected expression of phenazine biosynthesis genes. Expression of the *phzA2* (−1.6×, BH-adjusted *P* = 1.6e-4), *phzB2* (−2.3×,

bioRxiv preprint doi: https://doi.org/10.64898/2026.10.23.761465; this version posted October 31, 2026. The copyright holder for this preprint (which was not certified by peer review) is the author/funder, who has granted bioRxiv a license to display the preprint in perpetuity. It is made available under a CC-BY-NC-ND 4.0 International license.

BH-adjusted *P* = 7.5e-10), and *phzH* (−2.0×, BH-adjusted *P* = 4.5e-6) genes decreased, while *phzA1* (+1.4×, BH-adjusted *P* = 1.2e-2) of the duplicate operon increased. However, we did not observe differences in the production of pyocyanin (*m/z* 211.086 [M+H]), phenazine-1-carboxylic acid (*m/z* 225.0671 [M+H]), phenazine dicarboxylic acid (*m/z* 269.1755), or phenazine-1-carboxamide (*m/z* 224.0824) between *P. aeruginosa* wild type and Δ*pvdA* during coculture with *A. dolens* (**Fig. S6G-N**). Together, these data suggest that coculture with *A. dolens* may alter the carbon and sulfur sources used by *P. aeruginosa,* and affect production of the T6SS.

***A. dolens* stimulates production of extracellular virulence factors by *P. aeruginosa*.** Pyoverdine positively regulates production of the virulence factors exotoxin A (ToxA) and the PrpL serine protease in *P. aeruginosa* acting through the FpvA-FpvR-PvdS signaling cascade (51, 52). We hypothesized that coculture with *A. dolens* may also stimulate production of these virulence factors. Expression of the *toxA* (+1.4×, BH-adjusted *P* = 2.6e-2) and *toxR* (+1.6×, BH-adjusted *P* = 5.1e-6) regulator genes increased during coculture (**Fig. 6A**). However, the expression of *prpL* was unchanged (+1.10×, BH-adjusted *P* = 0.64).

We wanted to verify if these transcriptional changes corresponded to changes in the production of ToxA protein. We excised the agar near *P. aeruginosa* growing next to *A. dolens*, and extracted proteins. We then used untargeted liquid chromatography-tandem mass spectrometry (LC-MS^2) to identify these proteins. We detected 65 extracellular proteins. Note, though we took care not to disturb the *P. aeruginosa* streak when we excised the agar, we also detected cytoplasmic (n=1,451), cytoplasmic membrane (n=443), periplasmic (n=143), outer membrane (n=89), flagella (n=3), and proteins with unknown localization (n=449), which are likely derived from cell lysis (**Table S6** in the supplemental material). Across 2,633 proteins we detected in agar whose corresponding genes we also detected with

bioRxiv preprint doi: https://doi.org/10.64898/2026.10.23.761465; this version posted October 31, 2026. The copyright holder for this preprint (which was not certified by peer review) is the author/funder, who has granted bioRxiv a license to display the preprint in perpetuity. It is made available under a CC-BY-NC-ND 4.0 International license.

356 transcriptomics, we noted a weak correlation between the protein abundance and transcriptional fold
357 changes (Spearman ρ = 0.18, *P* = 1.8e-21).
358
359 In total, we identified 19 extracellular proteins that were present at higher levels during
360 coculture (**Fig. 7**). Specifically, production and/or secretion of extracellular virulence factors was
361 increased in coculture (Fisher's exact OR: 11.0, *P* = 3.4e-5). These virulence factors included AprA (+4.9×,
362 BH-adjusted *P* = 1.3e-3), LasB (+2.7×, BH-adjusted *P* = 1.2e-3), PaaP (+2.7×, BH-adjusted *P* =5.7e-3), PlcB
363 (+2.2×, BH-adjusted *P* = 1.3e-2), and ToxA (+2.2×, BH-adjusted *P* = 3.4e-3). In addition, the hemophore
364 HasAp (+4.4×, BH-adjusted *P* = 6.7e-3), which is known to be induced under iron-limiting conditions (53),
365 was present at higher levels during coculture. Three extracellular proteins were decreased in coculture,
366 including the S4 pyocin (−3.0×, BH-adjusted *P* = 1.2e-2). Taken together, our data indicate that *A. dolens*
367 modulates multiple iron-responsive pathways in *P. aeruginosa* and stimulates production of virulence
368 factors.
369

bioRxiv preprint doi: https://doi.org/10.64898/2026.10.23.761465; this version posted October 31, 2026. The copyright holder for this preprint (which was not certified by peer review) is the author/funder, who has granted bioRxiv a license to display the preprint in perpetuity. It is made available under a CC-BY-NC-ND 4.0 International license.

Discussion

In this study we investigated interactions between the CF pathogens *Achromobacter* spp. and *P. aeruginosa*. Using existing sequencing data, we confirmed that *Achromobacter-P. aeruginosa* coinfections are associated with more severe loss of lung function than infection with either of these pathogens alone. Critically, this effect was specific to *Achromobacter*, as coinfections with *P. aeruginosa* and other CF bacterial pathogens did not exacerbate lung function decline (**Fig. 1**). We then determined that *Achromobacter* spp. that are known to infect the airways of pwCF induced production of the siderophore and virulence factor pyoverdine when cocultured with *P. aeruginosa* (**Fig. 2** and **Fig. 3**). We found that this phenomenon occurred broadly, as *Achromobacter* induced pyoverdine in multiple clinical *Pseudomonas* isolates from pwCF (**Table 1**). We sequenced the genomes of the *Achromobacter* spp., and we tested and determined that most contained a BGC for the siderophore alcaligin (**Fig. 3**). We confirmed that during coculture *A. dolens* produces alcaligin and *P. aeruginosa* produces the siderophores pyoverdine and pyochelin (**Fig. 4**). We then determined that pyoverdine induction in coculture was dependent on iron (**Fig. 5**). Finally, we found that coculture with *A. dolens* stimulates expression and production of multiple virulence factors by *P. aeruginosa* (**Fig. 6** and **Fig. 7**).

Within the environment of the CF airway, iron is available via multiple sources. For instance, hemorrhage introduces heme into the airway, and proteolysis of transferrin and lactoferrin may release ferric iron (54). Furthermore, cultured airway epithelial cells that express ΔF508-CFTR release more iron into the apical medium than cells that express a fully functional CFTR (55). As one means to acquire this iron, microbes produce siderophores. Indeed, 17 siderophores from the CF airway microbiota have been reported, making them one of the most commonly described classes of secondary metabolites from CF microbes to date (56). Siderophore production is required for many pathogens to colonize and infect the

bioRxiv preprint doi: https://doi.org/10.64898/2026.10.23.761465; this version posted October 31, 2026. The copyright holder for this preprint (which was not certified by peer review) is the author/funder, who has granted bioRxiv a license to display the preprint in perpetuity. It is made available under a CC-BY-NC-ND 4.0 International license.

394 airway. For example, *B. pertussis fauA* mutants exhibit defects in murine lung colonization due to their
395 inability to import ferric alcaligin, and *B. bronchiseptica* alcaligin biosynthesis mutants display broad
396 colonization defects across the swine respiratory tract and cause less severe disease (38, 39). In the case
397 of *P. aeruginosa*, production of pyoverdine has been confirmed in the lungs of pwCF (57, 58) and
398 supports airway colonization (59–61). However, reliance on siderophores by *P. aeruginosa* changes over
399 the course of infection. Chronic infection isolates often harbor mutations in pyoverdine biosynthesis as
400 the source of iron in the CF airway changes (62). How changes in iron availability and siderophore
401 production influence competition between CF pathogens over the course of chronic infection remains
402 poorly understood, but our data suggest that these interactions may have important consequences for
403 disease.
404
405 Ferripyoverdine signaling through the FpvA-FpvR-PvdS signaling cascade promotes production of
406 pyoverdine and the virulence factors exotoxin A and PrpL (52). Unexpectedly, we did not observe
407 increased production of PrpL in *P. aeruginosa* during coculture with *A. dolens*. However, coculture with
408 *A. dolens* increased production of four additional secreted virulence factors (AprA, LasB, PaaP, and PlcP)
409 (**Fig. 7**). There are no FBS sequences upstream of the corresponding genes for these virulence factors.
410 We currently do not know how *A. dolens* induces their production. However, with the exception of *toxA*,
411 none of these genes were upregulated, suggesting post-transcriptional regulation.
412
413 Pyoverdine itself is cytotoxic toward macrophages, kills *Caenorhabditis elegans* directly, and
414 increases *P. aeruginosa* virulence in murine burn wound, endocarditis, and pneumonia models (63–67).
415 Consequently, under iron-limitation, *P. aeruginosa* becomes more virulent (68). Therefore, we
416 hypothesize that the lung function decline exacerbated during *Achromobacter-P. aeruginosa* coinfections
417 occur, in part, as a byproduct of exploitation competition for iron between these pathogens. Notably,

bioRxiv preprint doi: https://doi.org/10.64898/2026.10.23.761465; this version posted October 31, 2026. The copyright holder for this preprint (which was not certified by peer review) is the author/funder, who has granted bioRxiv a license to display the preprint in perpetuity. It is made available under a CC-BY-NC-ND 4.0 International license.

418 while alcaligin is a high-affinity iron chelator ($-\log_{10}[Fe^{3+}]_{Free}$ when $[Fe^{3+}]$ = 1 μM, [Siderophore] = 10 μM,
419 pH 7.4 [pFe]: 23), pyoverdine is four orders of magnitude stronger (pFe: 27) (41, 69). This does not
420 support a simple model in which alcaligin sequesters all available iron during competition and
421 completely starves *P. aeruginosa* of iron. Total iron starvation is likely not required to induce siderophore
422 production in *P. aeruginosa* as a response. In support of this idea, pyochelin (pFe: 16) (70) is a
423 substantially weaker siderophore than both alcaligin and pyoverdine. We detected increased pyochelin
424 production by Δ*pvdA* (compare **Fig. 4G** and **Fig. 4H**). If *A. dolens* depleted all available iron, then we
425 would expect complete growth inhibition of the Δ*pvdA* Δ*pchA* double mutant (**Fig. S5**). Instead, our data
426 suggest that iron limitation imposed in our coculture conditions is sufficient to alter *P. aeruginosa*
427 siderophore production without fully preventing growth. Within the spatially structured environment of
428 the CF airway, alcaligin could reduce local iron concentration sufficiently to induce pyoverdine (71–73). It
429 is tempting to speculate that increased severity of *Achromobacter-Pseudomonas* coinfections is due
430 solely to production of alcaligin as a relatively strong siderophore. However, the relative strengths of
431 siderophores produced by CF isolates *Burkholderia* spp., *S. aureus*, and *Stenotrophomonas maltophilia*
432 are not reported (74–81), making these comparisons impossible at this time.
433
434 Previous clinical studies (12) and the data we present suggest that *Achromobacter* increases *P.*
435 *aeruginosa* virulence. However, the opposite effect on virulence in zebrafish was recently reported (29).
436 Notably, these effects are strain-dependent, as Besse and Menetrey et al. found that strain Ax 200
437 reduced virulence, while the clonal strain Ax 198, isolated from the same patient, did not. Intriguingly,
438 these authors also report that production of the pyochelin receptor FptA by *P. aeruginosa* strain II.17
439 decreased during coculture with *A. xylosoxidans* strain Ax 200 and Fur decreased during coculture with
440 either strain Ax 198 or Ax 200. Similarly, pyoverdine production by II.17 was reduced during coculture
441 with either *A. xylosoxidans*. Together, these data led Besse and Menetry et al. to propose that iron

bioRxiv preprint doi: https://doi.org/10.64898/2026.10.23.761465; this version posted October 31, 2026. The copyright holder for this preprint (which was not certified by peer review) is the author/funder, who has granted bioRxiv a license to display the preprint in perpetuity. It is made available under a CC-BY-NC-ND 4.0 International license.

uptake by *P. aeruginosa* might be inhibited by *A. xylosoxidans* (29). These findings contrast with what we observed. It is not known if strains Ax 198 or Ax 200 produce alcaligin, but they do encode the *alc* BGC. We do note that four *A. xylosoxidans* strains we tested encode the *alc* BGC, but did not induce pyoverdine (**Fig. 3A**). It is possible that *A. xylosoxidans* strains Ax 198 and Ax 200, do not produce alcaligin. Regardless, the results of our experiments (**Figs. 6** and **7**), provide support for the idea that iron homeostasis is affected in *P. aeruginosa* during coculture with *A. dolens*.

Currently, our data suggest that alcaligin-imposed iron limitation induces pyoverdine production, but we have not directly demonstrated this mechanism. Thus far, our attempts to generate an alcaligin biosynthesis mutant in *A. dolens* strain RMS0405 have not been successful. Further, four strains of *A. xylosoxidans* encode *alc*, but do not induce pyoverdine in cocultured (**Fig. 3A**). We hypothesize that this discrepancy may be due to lack of alcaligin production. However, we have not identified any specific mutations in these strains that we would expect to impact alcaligin. In contrast, we observed that *Achromobacter* strain DSM 23807, *Achromobacter spanius* strain DSM 11386, and *A. xylosoxidans* strain DSM 26089 induce pyoverdine, but lack the *alc* BGC (**Fig. 3A**). In the case of *A. xylosoxidans* strain DSM 26089, we identified a BGC for a predicted non-ribosomal peptide metallophore, which is currently under investigation. However, we did not identify siderophore BGCs in *A. insolitus* or *A. spanius*. Perhaps these strains encode siderophores that we have not detected or there are alternative pathways to pyoverdine induction that remain to be discovered.

We last note an intriguing pattern we observed. The H1 T6SS genes had increased expression in *P. aeruginosa* during coculture, and this system functions broadly in interspecies bacterial competition (82). Conversely, the protein whose abundance decreased the most in coculture was pyocin S4. This protein resembles a colicin and that uses FpvA as its receptor for intraspecies competition (83). We

bioRxiv preprint doi: https://doi.org/10.64898/2026.10.23.761465; this version posted October 31, 2026. The copyright holder for this preprint (which was not certified by peer review) is the author/funder, who has granted bioRxiv a license to display the preprint in perpetuity. It is made available under a CC-BY-NC-ND 4.0 International license.

speculate that coculture with *A. dolens* could cause *P. aeruginosa* to repress pyocin S4 as expression of *fpvA* increases, shifting this pathogen from intraspecies to interspecies competition, as evidenced by increased expression of the H1 T6SS genes. Subsequent work will be required to investigate if coculture with *A. dolens* alters competitive phenotypes broadly in *P. aeruginosa*.

In conclusion, we report that *Achromobacter* spp. induce production of pyoverdine by *P. aeruginosa* during coculture. Pyoverdine is itself a virulence factor that also regulates production of other virulence factors. Our observation may serve to explain the basis underlying the increased severity of disease in pwCF that are coinfected with both of these pathogens. It is of note that this phenomenon is not limited to *Achromobacter*, as Herzog et al. recently demonstrated that another group of emerging CF pathogens, the *Pandoraea* spp., produce siderophores called pandorabactins that induce pyoverdine production in *P. aeruginosa* (84). Thus, the potential for increased virulence of *P. aeruginosa* in coinfections may be more common than previously appreciated.

bioRxiv preprint doi: https://doi.org/10.64898/2026.10.23.761465; this version posted October 31, 2026. The copyright holder for this preprint (which was not certified by peer review) is the author/funder, who has granted bioRxiv a license to display the preprint in perpetuity. It is made available under a CC-BY-NC-ND 4.0 International license.

Materials and Methods

***Achromobacter* and *Pseudomonas* coinfection analyses**. We previously described a reanalysis of 16S rRNA gene amplicon sequencing studies from CF airway samples (7). In the present study, we used these same data to assess the effects of coinfection with *Achromobacter* and *Pseudomonas* on lung function. Using a 1% relative abundance cutoff, we assigned samples to the following groups: no pathogen present, *Pseudomonas* only, *Achromobacter* only, or both pathogens. To confirm that the coinfection association was robust to the threshold used to define presence, we recomputed the difference in mean FEV_1 pp values between samples with both pathogens and samples without *Pseudomonas* nor *Achromobacter* across thresholds of 0.1, 0.5, 1, 2, and 5% relative abundance, and estimated each mean difference and its 95% CI with Welch's *t*-test. We excluded samples that lacked both *Pseudomonas* and *Achromobacter* but contained at least one other CF pathogen (*Burkholderia*, *Haemophilus*, *Staphylococcus*, or *Stenotrophomonas*), so that the no pathogen group was free of all six CF pathogens. We compared FEV_1 pp values among the groups using pairwise Wilcoxon rank-sum tests and adjusted *P*-values for multiple comparisons with the Benjamini-Hochberg (BH) false discovery rate. We defined severe disease as samples where the FEV1 pp value was ≤30%. To compare the burden of severe disease for each group, we estimated the proportion of severe samples and the 95% confidence interval (CI) with the exact binomial method. We compared each group to the both pathogens group using Fisher's exact test and adjusted the resulting *P*-values with the BH method.

To test whether lung function decline scaled with the degree of coinfection with *Achromobacter* and *Pseudomonas*, we related the combined relative abundance of *Achromobacter* and *Pseudomonas* to the FEV_1 pp value using Spearman's rank correlation. To test whether the association with worse lung function was specific to *Achromobacter*, we restricted the data to *Pseudomonas*-positive samples and fit

bioRxiv preprint doi: https://doi.org/10.64898/2026.10.23.761465; this version posted October 31, 2026. The copyright holder for this preprint (which was not certified by peer review) is the author/funder, who has granted bioRxiv a license to display the preprint in perpetuity. It is made available under a CC-BY-NC-ND 4.0 International license.

a single multivariable ordinary least-squares model, FEV_1 pp ~ *Achromobacter* + *Burkholderia* + *Haemophilus* + *Staphylococcus* + *Stenotrophomonas* + Age + BioProject Accession, in which each pathogen term was a binary indicator of presence (≥1% relative abundance). We interpreted each pathogen coefficient as the adjusted change in FEV_1 pp value associated with copresence of that pathogen, relative to *Pseudomonas*-positive samples lacking that pathogen and with the remaining pathogens held constant, and we report 95% CIs and per-coefficient *t*-test BH-adjusted *P*-values. We restricted this model to samples with complete covariate data.

Bacterial strains and media. The *Pseudomonas* isolates and *Achromobacter* strains used in this study are provided in **Tables S2 and S7**, respectively, in the supplemental material. For general propagation and manipulation, we used lysogeny broth (LB; 1.0% [wt/vol] tryptone, 0.5% [wt/vol] yeast extract, 0.5% [wt/vol] sodium chloride, 1 mM sodium hydroxide). All plates were solidified using 1.5% (wt/vol) agar. For coculture assays, we used SCFM (1.3 mM sodium dihydrogen phosphate, 1.25 mM disodium hydrogen phosphate, 0.35 mM potassium nitrate, 0.27 mM potassium sulfate, 2.3 mM ammonium chloride, 15 mM potassium chloride, 52 mM sodium chloride, 10 mM 3-(N-morpholino)propanesulfonic acid, 1.4 mM serine, 1.5 mM glutamate, 1.7 mM proline, 1.2 mM glycine, 1.8 mM alanine, 1.1 mM valine, 0.6 mM methionine, 1.1 mM isoleucine, 1.6 mM leucine, 0.7 mM ornithine, 2.1 mM lysine, 0.3 mM arginine, 0.01 mM tryptophan, 0.8 mM aspartate, 0.8 mM tyrosine, 1 mM threonine, 0.2 mM cysteine, 0.5 mM phenylalanine, 0.5 mM histidine, 3 mM glucose, 9 mM lactate, 0.6 mM magnesium chloride, 1.7 mM calcium chloride, 3.6 μM iron (II) sulfate, pH 6.8) (85). To make SCFM agar plates, we mixed 3% [wt/vol] agar with double-strength SCFM. We selected exconjugants during complementation of *P. aeruginosa* mutants using Vogel-Bonner minimal medium (VBMM; 0.02% [wt/vol] magnesium sulfate heptahydrate, 1% [wt/vol] dipotassium hydrogen phosphate, 0.2% [wt/vol] citric acid, 0.35% [wt/vol] ammonium sodium phosphate dibasic) agar plates containing tetracycline.

bioRxiv preprint doi: https://doi.org/10.64898/2026.10.23.761465; this version posted October 31, 2026. The copyright holder for this preprint (which was not certified by peer review) is the author/funder, who has granted bioRxiv a license to display the preprint in perpetuity. It is made available under a CC-BY-NC-ND 4.0 International license.

Identification of *Achromobacter* isolates. We isolated *A. dolens* strain RMS0405 as part of a previous study (7). Briefly, we used MacConkey agar (1.7% [wt/vol] gelatin peptone, 1.0% [wt/vol], sodium chloride, 0.15% [wt/vol] bile salts, 0.15% [wt/vol] casein peptone, 0.15% [wt/vol] meat peptone, 104 μM neutral red, 2.5 μM crystal violet, 1.35% [wt/vol] agar, pH 7.1) supplemented with 0.5% [wt/vol] xylose with the following additions after autoclaving: 20 μg/mL vancomycin, 20 μg/mL aztreonam, and 5 μg/mL amphotericin B (MCXVAA). We cultured bacterial strains in 3 mL of BHI (1.45% [wt/vol] casein peptone, 0.7% [wt/vol] meat peptone, 0.6% [wt/vol] brain heart infusion solids, 0.5% [wt/vol] sodium chloride, 0.25% [wt/vol] disodium phosphate, 0.2% [wt/vol] dextrose) in a shaker at 37°C. We extracted DNA from the overnight liquid culture using the phenol-chloroform extraction method. We amplified the full-length 16S rRNA gene using the universal primers 27F (5'-AGAGTTTGATCMTGGCTCAG-3') and 1492R (5'-CGGTTACCTTGTTACGACTT-3') and performed Sanger sequencing at the Oklahoma State University Genomics and Proteomics Center.

Cross-streak coculture assays. We inoculated 3 mL LB with single colonies of *Achromobacter* spp. isolates and incubated the cultures at 37°C overnight with shaking. We then adjusted the optical density at 600 nm (OD_{600}) of the overnight culture to 1.0 and spread 50 μL in a ~8 × ~1.5 cm-wide line in the center of a 25 mL SCFM agar plate (diameter: 8.6 cm). We incubated the plates for 72 h at 37°C. We prepared overnight (16 to 18 h) cultures of *P. aeruginosa* strains by inoculating single colonies into 3 mL LB. We diluted the overnight cultures to OD_{600} = 0.01. We then used sterilized wooden applicator sticks to streak the cultures perpendicularly to the *Achromobacter* spp. streak. We returned the plates to 37°C and assessed pyoverdine production after overnight incubation under blue light (λ = 470 nm) using a transilluminator.

bioRxiv preprint doi: https://doi.org/10.64898/2026.10.23.761465; this version posted October 31, 2026. The copyright holder for this preprint (which was not certified by peer review) is the author/funder, who has granted bioRxiv a license to display the preprint in perpetuity. It is made available under a CC-BY-NC-ND 4.0 International license.

552 **Genomic DNA extraction, sequencing, and assembly.** We extracted genomic DNA from *Achromobacter*
553 spp. using previously reported method (86). Briefly, we washed cell pellets from 3 ml of an overnight
554 culture in BHI broth in 1 ml of Buffer 1 (150 mM NaCl, 10 mM EDTA, 20 mM Tris-HCl, pH 8). We then
555 resuspended the cells in 1 mL of fresh Buffer 1 with 1 mg RNase A and SDS to a final concentration of
556 1.4% (wt/vol). We incubated the samples at 37°C for 90 min. We then added 0.4 mg of proteinase K and
557 incubated samples at 65°C for 20 min. We incubated samples at 37°C for 16 h to ensure complete lysis.
558 Subsequently, we extracted and purified genomic DNA used standard phenol-chloroform extraction and
559 followed by isopropanol precipitation.
560
561 We submitted genomic DNA from *A. dolens* strain RMS0405 and *A. xylosoxidans* DSM 26089 to
562 Plasmidsaurus for whole genome sequencing using Oxford Nanopore Technology. Libraries were
563 prepared using v14 library prep chemistry and sequenced using R10.4.1 flow cells. Bases were called
564 using Dorado v4.3 with default Q10 quality filtering (https://github.com/nanoporetech/dorado). Then
565 Filtlong v0.2.1 (https://github.com/rrwick/Filtlong) was used to remove reads <300 bp and retain the
566 95% highest quality reads. Subsequently, Autocycler (87) was used to generate assemblies using Flye
567 v2.9.6+ (88) and Hifiasm (89), remove low depth and small contigs, then compress, cluster, trim and,
568 resolve the assemblies. For all other *Achromobacter* spp., we submitted genomes to SeqCoast for whole
569 genome sequencing. Libraries were prepared with a single library preparation method based on the
570 Illumina Nextera kit and sequenced using the 2× 150-bp paired-end Illumina NextSeq 2000 platform at
571 SeqCoast. We processed raw genomic reads using fastp 0.23.2 (90) and assembled draft genome
572 sequences using SPAdes 3.15.5 (91), using default parameters for both. See **Table S7** in the supplemental
573 material for all genome sequencing statistics.
574

bioRxiv preprint doi: https://doi.org/10.64898/2026.10.23.761465; this version posted October 31, 2026. The copyright holder for this preprint (which was not certified by peer review) is the author/funder, who has granted bioRxiv a license to display the preprint in perpetuity. It is made available under a CC-BY-NC-ND 4.0 International license.

Detection, identification, and clustering of *Achromobacter* BGCs. We identified BGCs in *Achromobacter* spp. using antiSMASH 8.0.4 (92) with the following parameters: --cb-general --cb-knownclusters --cb-subclusters. To group the BGCs into GCFs, we used BiG-SCAPE 2.0.3 (93) with the following parameters: --mibig-version 4.0 --classify category --mix --include-singletons. We generated a heat map in R using complex Heatmap (94). We used clinker (95) to compare the *alc* BGCs from *Achromobacter* spp. to the reference BGC from *B. pertussis* strain Tohama I (https://mibig.secondarymetabolites.org/repository/BGC0002464.3/index.html).

Generating *pvdA* complement. We complemented the *pvdA* mutant via integration of *pvdA* using the mini-CTX1 plasmid (96). We amplified *pvdA* using primers oRMS125 (5'-ATGCGGATCCAATGGGAAGCCGACTGATTT-3') and oRMS116 (5'-ATGCGAATTCCATGCAACGAAAACGCCCTG-3'). These primers introduced BamHI and EcoRI restriction overhangs (underlined), respectively, which we used to introduce *pvdA* into mini-CTX-1. We then transformed the resulting plasmid into *Escherichia coli* SM10 for intergeneric conjugation into *P. aeruginosa*. We selected exconjugants using VBBM agar plates containing 75 µg/mL tetracycline. We passaged exconjugants onto LB plates with 25 µg/ml tetracycline. We confirmed complementation by observing exconjugants under blue light using a transilluminator to detect pyoverdine fluorescence and by PCR using primers oRMS117 (5'-CGCCCCTACGAAGGTACCGACA-3') and oRMS118 (5'-CGACGGCGGAGTTCAGCTGATA-3'), which anneal up- and downstream of the *attB* site, respectively.

Generating *pchA* deletion mutants. We deleted the *pchA* gene in *P. aeruginosa* strain PAO1 wild type and Δ*pvdA* using plasmid pEXG2-Δ*pchA* that was provided by Dr. Erika Lutter (Oklahoma State University). We performed intergeneric conjugation using *E. coli* SM10 using VBBM agar plates containing 60 µg/ml gentamicin. We then passaged exconjugants on LB with 15% (wt/vol) sucrose for

bioRxiv preprint doi: https://doi.org/10.64898/2026.10.23.761465; this version posted October 31, 2026. The copyright holder for this preprint (which was not certified by peer review) is the author/funder, who has granted bioRxiv a license to display the preprint in perpetuity. It is made available under a CC-BY-NC-ND 4.0 International license.

599 counterselection. We confirmed deletion of *pchA* using primers *pchA* seq F (5'-
600 CAGCGAGCTACTCGAGGACG-3') and *pchA* seq R (5'-GTCATGGCCCGTGGGGTTAA-3').
601
602 **MALDI-QqTOF-MSI**. We cocultured *A. dolens* and three spots *P. aeruginosa* on 10 mL SCFM with 25 μM
603 $FeCl_3$ agar plates at 37°C for 24 h. Following incubation, we excised the coculture from the plate using a
604 sterile razor blade and transferred it to a ground stainless steel MALDI target plate, ensuring that no air
605 bubbles formed between the plate and agar. Afterwards we applied a 1:1 mixture of α-cyano-4-
606 hydroxycinnamic acid and 2,5-dihydroxybenzoic acid (CHCA:DHB) MALDI matrix with a 53-micron
607 stainless steel sieve. We dried the plates at 37°C for 4 h using a homemade spinning apparatus (97).
608 Subsequently, we removed excess MALDI matrix using compressed air. We spotted 1 μL of saturated red
609 phosphorous in 50% (vol/vol) acetonitrile as a calibrant and allowed it to dry. We performed acquisition
610 on a timsTOF flex (Bruker Daltonics) using timsControl v6.0.3_abe6ecc8_1 and flexImaging v7.5 in
611 positive mode at a lateral resolution of 200 µm. We provide the method parameters in **Table S8** in the
612 supplemental material. We analyzed the resulting .slx files using SCiLS Lab v2026b core. We applied total
613 ion count (TIC) normalization. We set the interval width to ± 4.6 ppm for the resulting ion images and
614 chose peak area as the Interval Processing Mode. We generated the ion image using Toggle Image Blend
615 Mode. All analyses were done in biological duplicate.
616
617 **MALDI-QqTOF-DDA-MS^2.** Following incubation as above, we spotted a single colony of *A. dolens* or *P.*
618 *aeruginosa* from each coculture onto a ground stainless steel MALDI target plate using a sterile
619 toothpick. Immediately after drying, we spotted 1 µL of a 1:1 mixture of CHCA:DHB MALDI matrix with
620 0.1% (vol/vol) trifluoroacetic acid on top of each colony. We performed acquisition on the same
621 instrument as above. After performing a first scan per each culture spot, we used the resulting .run file
622 to generate a precursor list using flex_MSMS_AutoXecute_Generator.exe (98). We then used the

bioRxiv preprint doi: https://doi.org/10.64898/2026.10.23.761465; this version posted October 31, 2026. The copyright holder for this preprint (which was not certified by peer review) is the author/funder, who has granted bioRxiv a license to display the preprint in perpetuity. It is made available under a CC-BY-NC-ND 4.0 International license.

resulting list of 100 precursors, not including the media or the matrix, to schedule DDA at the MS^2 level. We provide the method parameters in **Table S9** in the supplemental material. We converted the resulting .d files to .mzML files using MSConvert (99) with PeakPicking on the MS level = 1 – 2 and uploaded to GNPS2 (100) for generation of molecular networks. We merged single MS^2 spectra and converted them to .mgf files using MZmine 3 v4.8.30 (101) and analyzed the resulting files with SIRIUS 4 v6.3.3 (102) for putative annotation of observed signals. All analyses were done using three individual colonies as biological replicates.

Transcriptomic comparison. We cultured *P. aeruginosa* strain PAO1 monocultures and cocultures with *A. dolens* strain RMS0405 on SCFM + 25 μM $FeCl_3$, as above. After 12 h coculture, we used a sterile 1 μL inoculation loop to collect *P. aeruginosa* biomass next to *A. dolens* or an equivalent amount of biomass from monoculture control plates. We resuspended the biomass in 100 μL TE buffer containing 50 mg/mL lysozyme and incubated the sample at 37°C for 30 min, with vortexing at 10 min intervals. We then added 150 μL of Monarch StabiLyse DNA/RNA buffer (NEB) and mixed the samples vigorously. We centrifuged the samples at 16,000 × g for 2 min at ambient temperature. We then extracted RNA from the supernatant using a Monarch Spin RNA Isolation Kit (NEB), following the manufacturer's instructions. We submitted RNA samples to the Oklahoma State University Microbiomics and Culturomics Core Facility (MCCF). RNA integrity and quality were determined using an Agilent RNA ScreenTape system on a TapeStation 4200, and RNA concentration was determined using the Qubit RNA Broad Range Assay Kit (Invitrogen). RNA-seq libraries were then prepared using the Zymo-Seq RiboFree Total RNA Library Kit (Zymo Research). The samples were then sequenced on an Illumina NextSeq 2000 platform using a NextSeq 2000 P3 100-cycle kit in a paired-end 2 × 50 bp configuration in the Oklahoma State University Next Generation Sequencing Core Facility. A library pool at a concentration of 740 pM was loaded for sequencing, with 5% PhiX included as a positive control.

bioRxiv preprint doi: https://doi.org/10.64898/2026.10.23.761465; this version posted October 31, 2026. The copyright holder for this preprint (which was not certified by peer review) is the author/funder, who has granted bioRxiv a license to display the preprint in perpetuity. It is made available under a CC-BY-NC-ND 4.0 International license.

We trimmed reads with fastp 0.23.2 and used kallisto 0.52.0 (103) to pseudoalign reads against a *k* = 31 index built from *P. aeruginosa* strain PAO1 coding sequencing using 100 bootstrap replicates. We used tximport 1.34.0 to import the abundances for testing differential expression with DESeq2 1.46.0 (104). We retained all genes with a pseudocount ≥10. We used apeglm 1.28.0 (105) to shrink the $\log_2$ fold changes for ranking and display. We assessed significance using a Wald test on the original $\log_2$ fold changes using a BH-adjusted *P*-value threshold of 0.05 for significance. To identify potential FBS sequences within promoters, we built a position weight matrix with MEME (106) in MEME suite 5.5.9 from 26 experimentally confirmed *P. aeruginosa* FBS. We then scanned from 300 bp upstream of start codons down to 50 bp within coding sequences for the presence of this sequence motif using fimo with a *P*-value threshold of 10^{-4}. We compared the proportion of genes with FBS enriched in each culture condition using a jackknife approach where we left one sample out of each analysis. We tested gene set enrichment using a combination of PseudoCAP categories along with some manually curated gene sets using a one-sided Fisher's exact test with Haldane-Anscombe-corrected OR and BH-adjusted *P*-values.

Proteome comparison. We used a protocol we previously employed to extract proteins embedded in agar (107). Briefly, we cultured *P. aeruginosa* strain PAO1 monocultures and cocultures with *A. dolens* strain RMS0405 on SCFM + 25 μM $FeCl_3$, as above. After 24 h coculture, we used clean razor blades to excise the agar ~0.1 cm from the *P. aeruginosa* streaks, without disturbing the bacterial growth. We centrifuged the agar slices at 4,000 × g for 10 min at ambient temperature and then combined them with an equal volume of extraction buffer (50 mM Tric-HCl, 0.2% [wt/vol], 0.2% [wt/vol] *N*-lauroylsarcosine sodium salt, pH 7.5), and incubated the mixture on a shaking platform at 150 RPM overnight. We then centrifuged the samples at 4,000 × g for 20 min at ambient temperature and filtered the supernatant through cheesecloth to remove agar. We added trichloroacetic acid to a final concentration of 7.5%

bioRxiv preprint doi: https://doi.org/10.64898/2026.10.23.761465; this version posted October 31, 2026. The copyright holder for this preprint (which was not certified by peer review) is the author/funder, who has granted bioRxiv a license to display the preprint in perpetuity. It is made available under a CC-BY-NC-ND 4.0 International license.

(wt/vol), precipitated protein at −20 °C overnight, and pelleted the precipirated protein by centrifuging the samples at 4,000 × g for 20 min at 4 °C.

The protein pellets were washed three times with cold acetone and resuspended in 150 μL of 5% (wt/vol) sodium dodecyl sulfate (SDS) in 100 mM Triethylammonium bicarbonate (TEAB) (pH 8). The samples were sonicated for 10 min in a refrigerated ultrasonic bath, centrifuged at 16,000 × g for 10 min at 4 °C, and the supernatant was transferred to a clean tube. After quantification using a bicinchoninic acid assay, 50 µg of protein was then transferred to a clean tube and reduced with 10 mM tris(2-carboxyethyl)phosphine at for 15 min at 55 °C. The reduced proteins were then alkylated with 40 mM iodoacetamide in the dark for 10 min and then acidified by adding 11 μL of 27.5% (wt/vol) phosphoric acid. The proteins were precipitated after addition of 913 μL S-Trap binding buffer (90% [vol/vol] methanol with 100 mM TEAB, pH 8) and loaded into an S-Trap Spin column. Then, 40 μL of 50 mM TEAB (pH 8) containing 1 µg MS-grade trypsin/LysC was added and incubated overnight at 37 °C . The peptides were eluted following the manufacturer's protocol, dried *in vacuo*, and reconstituted in 200 µL using 0.1% (vol/vol) trifluoroacetic acid (TFA).

Subsequently, the peptides were desalted using a C18 peptide desalting spin column equilibrated with a 3% (vol/vol) acetonitrile (ACN) and 0.1% (vol/vol) TFA solution. The bound peptides were washed with the same solution to remove salts and other hydrophilic contaminants before being eluted using a 60% (vol/vol) ACN and 0.1% (vol/vol) TFA solution. The eluted proteins were dried *in vacuo* and reconstituted in 0.1% (vol/vol) formic acid. The peptides were injected onto a 75 µm × 50 cm nano-HPLC column packed with 1.9 µm C18 particles and connected to an Easy-nLC 1200 nano-HPLC system. Peptides were separated by gradient chromatography using 0.1% aqueous formic acid as mobile phase A and 80:20:0.1 ACN/water/formic acid as mobile phase B. Peptide separation was performed

bioRxiv preprint doi: https://doi.org/10.64898/2026.10.23.761465; this version posted October 31, 2026. The copyright holder for this preprint (which was not certified by peer review) is the author/funder, who has granted bioRxiv a license to display the preprint in perpetuity. It is made available under a CC-BY-NC-ND 4.0 International license.

using a gradient of 4–32% mobile phase B over 120 min at a flow rate of 250 nL per min. The eluted peptides were ionized using a Nanospray Flex ion source and analyzed on an Orbitrap Fusion Tribrid mass spectrometer (Thermo Fisher Scientific). Mass spectrometric data were acquired in DDA mode using a top-speed scan cycle. Full MS scans were acquired in the Orbitrap, followed by quadrupole selection of precursor ions, higher-energy collisional dissociation (HCD), and MS^2 analysis of fragment ions in the ion trap.

Raw mass spectrometry files were processed using MaxQuant v2.0.2.0 (108) and searched against the *P. aeruginosa* proteome from the UniProt (accession: UP000002438). The Database searching was performed using standard MaxQuant parameters, with trypsin/P specified as the proteolytic enzyme and up to two missed cleavages allowed. Peptide-spectrum matches and protein identifications were filtered at a false discovery rate (FDR) of 1%. In total, we analyzed the proteomes from two biological replicates with three technical replicates.

We filtered the protein groups from MaxQuant to remove any matches to a decoy database, potential contaminants, and proteins identified with only a modified peptide. We only retained proteins with at least one non-zero label-free quantification (LFQ) intensity and at least two MS^2 counts. We replaced zero LFQ values with the 1st percentile of the measured LFQ value within a sample. All samples within a biological replicate (three cocultures and three monocultures) were processed together for proteomics, but the two biological replicates were processed and analyzed by mass spectrometry in two separate runs. We accounted for batch effects by fitting each protein with its $\log_2$ LFQ ~ intercept + condition + batch. We tested condition coefficients using a two-sided *t*-test on the residual degrees of freedom. We adjusted *P*-values using the BH procedure. We classified proteins as extracellular based on curation of the subcellular localization assignments from the *Pseudomonas* Genome Database (109).

bioRxiv preprint doi: https://doi.org/10.64898/2026.10.23.761465; this version posted October 31, 2026. The copyright holder for this preprint (which was not certified by peer review) is the author/funder, who has granted bioRxiv a license to display the preprint in perpetuity. It is made available under a CC-BY-NC-ND 4.0 International license.

719

720 **Statistical analysis and data visualization**. We performed all statistical analyses in R with specific
721 packages as described in the preceding sections. We generated graphics using ggplot2 (110) with some
722 cleanup and figure assembly in InkScape.

723

724 **Data availability**. The raw reads and genome sequences of *Achromobacter* spp. generated during this
725 study have been deposited under BioProject Accession number PRJNA1544629. All MALDI-QqTOF-MSI
726 datasets are deposited at MassIVE under accession MSV000102382. All transcriptomic raw reads are
727 deposited under BioProject Accession number PRJNA1545112. All other raw data and derived data are
728 available at https://doi.org/10.6084/m9.figshare.34702161. The scripts necessary to replicate this work
729 are available at https://github.com/reedstubbendieck/Achromobacter_Pseudomonas_Interactions.

730

bioRxiv preprint doi: https://doi.org/10.64898/2026.10.23.761465; this version posted October 31, 2026. The copyright holder for this preprint (which was not certified by peer review) is the author/funder, who has granted bioRxiv a license to display the preprint in perpetuity. It is made available under a CC-BY-NC-ND 4.0 International license.

731

732 **Acknowledgements**

733

734 We thank Sandra Armstrong (University of Minnesota) for generous insight into alcaligin. We thank
735 Matthew Cabeen (Oklahoma State University [OSU]), Ryan Hunter (State University of New York at
736 Buffalo), Erika Lutter (OSU), and Avishek Mitra (OSU) for strains. We thank Yingxin Zhang (OSU) for
737 assistance with deletion of *pchA*. We thank Mostafa Elshahed and Aymen Yassir (OSU Microbiomics and
738 Culturomics Core Facility) for assistance with transcriptomics (P20 GM152333). We thank Uma Aryal
739 (OSU) and Ali Ali (OSU) for assistance with proteomics.

740

741 This research was supported by the National Institute of General Medical Sciences Centers of
742 Biomedical Research Excellence program (P20 GM152333) to R.M.S. L.R.V. was supported by the 2024
743 Activating Innovative Graduate Research Award (AIGRA) at the University of California, Santa Cruz. The
744 funders had no role in study design, data collection and interpretation, or the decision to submit the
745 work for publication.

746

bioRxiv preprint doi: https://doi.org/10.64898/2026.10.23.761465; this version posted October 31, 2026. The copyright holder for this preprint (which was not certified by peer review) is the author/funder, who has granted bioRxiv a license to display the preprint in perpetuity. It is made available under a CC-BY-NC-ND 4.0 International license.

Author Contributions

Conceptualization: Niladri Bhowmik and Reed M. Stubbendieck

Data Curation: Niladri Bhowmik, Laura Rodriguez-Velandia, Laura M. Sanchez, Reed M. Stubbendieck

Formal analysis: Niladri Bhowmik, Laura Rodriguez-Velandia, Laura M. Sanchez, and Reed M. Stubbendieck

Funding acquisition: Laura Rodriguez-Velandia and Reed M. Stubbendieck

Investigation: Niladri Bhowmik, Laura Rodriguez-Velandia, Mercedes Pérez Pérez, Sydney M. Morabbi, Laura M. Sanchez, and Reed M. Stubbendieck

Resources: Reed M. Stubbendieck

Supervision: Laura M. Sanchez and Reed M. Stubbendieck

Visualization: Niladri Bhowmik, Laura Rodriguez-Velandia, and Reed M. Stubbendieck

Writing – original draft: Niladri Bhowmik and Reed M. Stubbendieck

bioRxiv preprint doi: https://doi.org/10.64898/2026.10.23.761465; this version posted October 31, 2026. The copyright holder for this preprint (which was not certified by peer review) is the author/funder, who has granted bioRxiv a license to display the preprint in perpetuity. It is made available under a CC-BY-NC-ND 4.0 International license.

760 **References**

761

762 1. Ehre C, Hansson GC, Thornton DJ, Ostedgaard LS. 2022. Mucus aberrant properties in CF: Insights
763 from cells and animal models. J Cyst Fibros S1569-1993(22)00656–7.

764 2. Guo J, Garratt A, Hill A. 2022. Worldwide rates of diagnosis and effective treatment for cystic
765 fibrosis. Journal of cystic fibrosis : official journal of the European Cystic Fibrosis Society
766 https://doi.org/10.1016/j.jcf.2022.01.009.

767 3. Singh H, Jani C, Marshall DC, Franco R, Bhatt P, Podder S, Shalhoub J, Kurman JS, Nanchal R, Uluer
768 AZ, Salciccioli JD. 2023. Cystic fibrosis-related mortality in the United States from 1999 to 2020: an
769 observational analysis of time trends and disparities. Sci Rep 13:15030.

770 4. Guss AM, Roeselers G, Newton ILG, Young CR, Klepac-Ceraj V, Lory S, Cavanaugh CM. 2011.
771 Phylogenetic and metabolic diversity of bacteria associated with cystic fibrosis. The ISME Journal
772 5:20–29.

773 5. Coburn B, Wang PW, Diaz Caballero J, Clark ST, Brahma V, Donaldson S, Zhang Y, Surendra A, Gong
774 Y, Elizabeth Tullis D, Yau YCW, Waters VJ, Hwang DM, Guttman DS. 2015. Lung microbiota across age
775 and disease stage in cystic fibrosis. Sci Rep 5:10241.

776 6. Adekoya AE, Kargbo HA, Ibberson CB. 2023. Defining microbial community functions in chronic
777 human infection with metatranscriptomics. mSystems 8:e0059323.

778 7. Morabbi SM, Bhowmik N, Sutherland S, Wylie EA, Decker RS, Al Daerwish A, Pérez Pérez M, Pascual
779 E, Lutter EI, Philmus B, Stubbendieck RM. 2026. Differential Metabolite Production Underlies

bioRxiv preprint doi: https://doi.org/10.64898/2026.10.23.761465; this version posted October 31, 2026. The copyright holder for this preprint (which was not certified by peer review) is the author/funder, who has granted bioRxiv a license to display the preprint in perpetuity. It is made available under a CC-BY-NC-ND 4.0 International license.

Disruption of the Cystic Fibrosis Airway Microbiota by Pathogens. bioRxiv https://doi.org/10.64898/2026.07.16.738945.

8. Filkins LM, Graber JA, Olson DG, Dolben EL, Lynd LR, Bhuju S, O'Toole GA. 2015. Coculture of Staphylococcus aureus with Pseudomonas aeruginosa Drives S. aureus towards Fermentative Metabolism and Reduced Viability in a Cystic Fibrosis Model. Journal of bacteriology 197:2252–64.

9. Fugère A, Lalonde Séguin D, Mitchell G, Déziel E, Dekimpe V, Cantin AM, Frost E, Malouin F. 2014. Interspecific small molecule interactions between clinical isolates of Pseudomonas aeruginosa and Staphylococcus aureus from adult cystic fibrosis patients. PLoS One 9:e86705.

10. Jenul C, Keim KC, Jens JN, Zeiler MJ, Schilcher K, Schurr MJ, Melander C, Phelan VV, Horswill AR. 2023. Pyochelin biotransformation by Staphylococcus aureus shapes bacterial competition with Pseudomonas aeruginosa in polymicrobial infections. Cell Rep 42:112540.

11. Liu Y, McQuillen EA, Rana PSJB, Gloag ES, Parsek MR, Wozniak DJ. 2024. A bacterial pigment provides cross-species protection from H2O2- and neutrophil-mediated killing. Proc Natl Acad Sci U S A 121:e2312334121.

12. Bhowmik N, Stubbendieck RM. 2025. Achromobacter spp.: Emerging pathogens in the cystic fibrosis lung. PLoS Pathog 21:e1013067.

13. Spilker T, Vandamme P, Lipuma JJ. 2013. Identification and distribution of Achromobacter species in cystic fibrosis. J Cyst Fibros 12:298–301.

14. Jeukens J, Freschi L, Vincent AT, Emond-Rheault J-G, Kukavica-Ibrulj I, Charette SJ, Levesque RC. 2017. A Pan-Genomic Approach to Understand the Basis of Host Adaptation in Achromobacter. Genome Biology and Evolution 9:1030–1046.

bioRxiv preprint doi: https://doi.org/10.64898/2026.10.23.761465; this version posted October 31, 2026. The copyright holder for this preprint (which was not certified by peer review) is the author/funder, who has granted bioRxiv a license to display the preprint in perpetuity. It is made available under a CC-BY-NC-ND 4.0 International license.

15. Veschetti L, Boaretti M, Saitta GM, Passarelli Mantovani R, Lleò MM, Sandri A, Malerba G. 2022. Achromobacter spp. prevalence and adaptation in cystic fibrosis lung infection. Microbiological Research 263:127140.

16. Lambiase A, Catania MR, Del Pezzo M, Rossano F, Terlizzi V, Sepe A, Raia V. 2011. Achromobacter xylosoxidans respiratory tract infection in cystic fibrosis patients. Eur J Clin Microbiol Infect Dis 30:973–980.

17. Recio R, Brañas P, Martínez MT, Chaves F, Orellana MA. 2018. Effect of respiratory Achromobacter spp. infection on pulmonary function in patients with cystic fibrosis. J Med Microbiol 67:952–956.

18. Vongthilath R, Richaud Thiriez B, Dehillotte C, Lemonnier L, Guillien A, Degano B, Dalphin M-L, Dalphin J-C, Plésiat P. 2019. Clinical and microbiological characteristics of cystic fibrosis adults never colonized by Pseudomonas aeruginosa: Analysis of the French CF registry. PLoS One 14:e0210201.

19. Marsac C, Berdah L, Thouvenin G, Sermet-Gaudelus I, Corvol H. 2021. Achromobacter xylosoxidans airway infection is associated with lung disease severity in children with cystic fibrosis. ERJ Open Res 7:00076–02021.

20. Turton K, Parks HJ, Zarodkiewicz P, Hamad MA, Dwane R, Parau G, Ingram RJ, Coll RC, Bryant CE, Valvano MA. 2023. The Achromobacter type 3 secretion system drives pyroptosis and immunopathology via independent activation of NLRC4 and NLRP3 inflammasomes. Cell Rep 42:113012.

21. Sahl C, Baumgarten M, Shannon O, Påhlman LI. 2023. Exoproducts of the Most Common Achromobacter Species in Cystic Fibrosis Evoke Similar Inflammatory Responses In Vitro. Microbiol Spectr 11:e0019523.

bioRxiv preprint doi: https://doi.org/10.64898/2026.10.23.761465; this version posted October 31, 2026. The copyright holder for this preprint (which was not certified by peer review) is the author/funder, who has granted bioRxiv a license to display the preprint in perpetuity. It is made available under a CC-BY-NC-ND 4.0 International license.

822 22. Sorlin P, Brivet E, Jean-Pierre V, Aujoulat F, Besse A, Dupont C, Chiron R, Jumas-Bilak E, Menetrey Q,
823 Marchandin H. 2024. Prevalence and variability of siderophore production in the Achromobacter
824 genus. Microbiol Spectr 12:e0295323.

825 23. Kerem E, Orenti A, Zolin A, Annicchiarico L, Drevinek P, ECFSPR with the list of contributing authors.
826 2023. Clinical outcomes associated with Achromobacter species infection in people with cystic
827 fibrosis. J Cyst Fibros 22:334–343.

828 24. Middleton PG, Mall MA, Dřevínek P, Lands LC, McKone EF, Polineni D, Ramsey BW, Taylor-Cousar JL,
829 Tullis E, Vermeulen F, Marigowda G, McKee CM, Moskowitz SM, Nair N, Savage J, Simard C, Tian S,
830 Waltz D, Xuan F, Rowe SM, Jain R. 2019. Elexacaftor–Tezacaftor–Ivacaftor for Cystic Fibrosis with a
831 Single Phe508del Allele. N Engl J Med 381:1809–1819.

832 25. Fajac I, Sermet I. 2021. Therapeutic Approaches for Patients with Cystic Fibrosis Not Eligible for
833 Current CFTR Modulators. Cells 10:2793.

834 26. Chalhoub H, Kampmeier S, Kahl BC, Van Bambeke F. 2022. Role of Efflux in Antibiotic Resistance of
835 Achromobacter xylosoxidans and Achromobacter insuavis Isolates From Patients With Cystic
836 Fibrosis. Front Microbiol 13:762307.

837 27. Tetart M, Wallet F, Kyheng M, Leroy S, Perez T, Le Rouzic O, Wallaert B, Prevotat A. 2019. Impact of
838 Achromobacter xylosoxidans isolation on the respiratory function of adult patients with cystic
839 fibrosis. ERJ Open Res 5:00051–02019.

840 28. Menetrey Q, Dupont C, Chiron R, Jumas-Bilak E, Marchandin H. 2020. High Occurrence of Bacterial
841 Competition Among Clinically Documented Opportunistic Pathogens Including Achromobacter
842 xylosoxidans in Cystic Fibrosis. Front Microbiol 11:558160.

bioRxiv preprint doi: https://doi.org/10.64898/2026.10.23.761465; this version posted October 31, 2026. The copyright holder for this preprint (which was not certified by peer review) is the author/funder, who has granted bioRxiv a license to display the preprint in perpetuity. It is made available under a CC-BY-NC-ND 4.0 International license.

29. Besse A, Menetrey Q, Jean-Pierre V, Huc-Brandt S, Aujoulat F, Dupont C, Chiron R, Armengaud J, Jumas-Bilak E, Molle V, Grenga L, Marchandin H. 2025. Achromobacter xylosoxidans modulates Pseudomonas aeruginosa virulence through a complex multi-target competition. Sci Rep 15:23392.

30. Sahl C, Andersson A, Larsson N, Paulsson M, Shannon O, Påhlman LI. 2025. The cystic fibrosis pathogen Achromobacter xylosoxidans inhibits biofilm formation of Pseudomonas aeruginosa. J Med Microbiol 74:002051.

31. Soh EY-C, Chhabra SR, Halliday N, Heeb S, Müller C, Birmes FS, Fetzner S, Cámara M, Chan K-G, Williams P. 2015. Biotic inactivation of the Pseudomonas aeruginosa quinolone signal molecule. Environmental Microbiology 17:4352–4365.

32. Lin J, Cheng J, Wang Y, Shen X. 2018. The Pseudomonas Quinolone Signal (PQS): Not Just for Quorum Sensing Anymore. Front Cell Infect Microbiol 8:230.

33. Johnson JS, Spakowicz DJ, Hong B-Y, Petersen LM, Demkowicz P, Chen L, Leopold SR, Hanson BM, Agresta HO, Gerstein M, Sodergren E, Weinstock GM. 2019. Evaluation of 16S rRNA gene sequencing for species and strain-level microbiome analysis. Nat Commun 10:5029.

34. Hassler HB, Probert B, Moore C, Lawson E, Jackson RW, Russell BT, Richards VP. 2022. Phylogenies of the 16S rRNA gene and its hypervariable regions lack concordance with core genome phylogenies. Microbiome 10:104.

35. Hunter RC, Asfour F, Dingemans J, Osuna BL, Samad T, Malfroot A, Cornelis P, Newman DK. 2013. Ferrous iron is a significant component of bioavailable iron in cystic fibrosis airways. mBio 4:e00557-13.

bioRxiv preprint doi: https://doi.org/10.64898/2026.10.23.761465; this version posted October 31, 2026. The copyright holder for this preprint (which was not certified by peer review) is the author/funder, who has granted bioRxiv a license to display the preprint in perpetuity. It is made available under a CC-BY-NC-ND 4.0 International license.

863 36. Reid DW, Withers NJ, Francis L, Wilson JW, Kotsimbos TC. 2002. Iron Deficiency in Cystic Fibrosis.
864 Chest 121:48–54.

865 37. Grace A, Sahu R, Owen DR, Dennis VA. 2022. Pseudomonas aeruginosa reference strains PAO1 and
866 PA14: A genomic, phenotypic, and therapeutic review. Front Microbiol 13:1023523.

867 38. Register KB, Ducey TF, Brockmeier SL, Dyer DW. 2001. Reduced virulence of a Bordetella
868 bronchiseptica siderophore mutant in neonatal swine. Infect Immun 69:2137–2143.

869 39. Brickman TJ, Armstrong SK. 2007. Impact of alcaligin siderophore utilization on in vivo growth of
870 Bordetella pertussis. Infect Immun 75:5305–5312.

871 40. Nishio T, Ishida Y. 1990. Production of Dihydroxamate Siderophore Alcaligin by *Alcaligenes*
872 *xylosoxidans* subsp. *xylosoxidans*. Agricultural and Biological Chemistry 54:1837–1839.

873 41. Hou Z, Sunderland CJ, Nishio T, Raymond KN. 1996. Preorganization of Ferric Alcaligin, Fe_2 L_3 . The
874 First Structure of a Ferric Dihydroxamate Siderophore. J Am Chem Soc 118:5148–5149.

875 42. Beaumont FC, Kang HY, Brickman TJ, Armstrong SK. 1998. Identification and characterization of
876 alcR, a gene encoding an AraC-like regulator of alcaligin siderophore biosynthesis and transport in
877 Bordetella pertussis and Bordetella bronchiseptica. J Bacteriol 180:862–870.

878 43. Pradel E, Guiso N, Locht C. 1998. Identification of AlcR, an AraC-type regulator of alcaligin
879 siderophore synthesis in Bordetella bronchiseptica and Bordetella pertussis. J Bacteriol 180:871–
880 880.

881 44. Brickman TJ, Kang HY, Armstrong SK. 2001. Transcriptional activation of Bordetella alcaligin
882 siderophore genes requires the AlcR regulator with alcaligin as inducer. J Bacteriol 183:483–489.

bioRxiv preprint doi: https://doi.org/10.64898/2026.10.23.761465; this version posted October 31, 2026. The copyright holder for this preprint (which was not certified by peer review) is the author/funder, who has granted bioRxiv a license to display the preprint in perpetuity. It is made available under a CC-BY-NC-ND 4.0 International license.

883 45. Brickman TJ, Armstrong SK. 2005. Bordetella AlcS transporter functions in alcaligin siderophore
884 export and is central to inducer sensing in positive regulation of alcaligin system gene expression. J
885 Bacteriol 187:3650–3661.

886 46. Brickman TJ, Armstrong SK. 1999. Essential role of the iron-regulated outer membrane receptor
887 FauA in alcaligin siderophore-mediated iron uptake in Bordetella species. J Bacteriol 181:5958–
888 5966.

889 47. Schwyn B, Neilands JB. 1987. Universal chemical assay for the detection and determination of
890 siderophores. Analytical biochemistry 160:47–56.

891 48. Neve RL, Carrillo BD, Phelan VV. 2021. Impact of artificial sputum media formulation on
892 Pseudomonas aeruginosa secondary metabolite production. Journal of bacteriology JB0025021.

893 49. Alontaga AY, Rodriguez JC, Schönbrunn E, Becker A, Funke T, Yukl ET, Hayashi T, Stobaugh J,
894 Moënne-Loccoz P, Rivera M. 2009. Structural Characterization of the Hemophore HasAp from
895 *Pseudomonas aeruginosa* : NMR Spectroscopy Reveals Protein−Protein Interactions between Holo-
896 HasAp and Hemoglobin†. Biochemistry 48:96–109.

897 50. Hood RD, Singh P, Hsu F, Güvener T, Carl MA, Trinidad RRS, Silverman JM, Ohlson BB, Hicks KG,
898 Plemel RL, Li M, Schwarz S, Wang WY, Merz AJ, Goodlett DR, Mougous JD. 2010. A type VI secretion
899 system of Pseudomonas aeruginosa targets a toxin to bacteria. Cell host & microbe 7:25–37.

900 51. Hunt TA, Peng W-T, Loubens I, Storey DG. 2002. The Pseudomonas aeruginosa alternative sigma
901 factor PvdS controls exotoxin A expression and is expressed in lung infections associated with cystic
902 fibrosis. Microbiology 148:3183–3193.

bioRxiv preprint doi: https://doi.org/10.64898/2026.10.23.761465; this version posted October 31, 2026. The copyright holder for this preprint (which was not certified by peer review) is the author/funder, who has granted bioRxiv a license to display the preprint in perpetuity. It is made available under a CC-BY-NC-ND 4.0 International license.

903 52. Lamont IL, Beare PA, Ochsner U, Vasil AI, Vasil ML. 2002. Siderophore-mediated signaling regulates
904 virulence factor production in *Pseudomonas aeruginosa*. Proc Natl Acad Sci USA 99:7072–7077.

905 53. Létoffé S, Redeker V, Wandersman C. 1998. Isolation and characterization of an extracellular haem-
906 binding protein from *Pseudomonas aeruginosa* that shares function and sequence similarities with
907 the *Serratia marcescens* HasA haemophore. Molecular Microbiology 28:1223–1234.

908 54. Reid DW, Anderson GJ, Lamont IL. 2009. Role of lung iron in determining the bacterial and host
909 struggle in cystic fibrosis. American Journal of Physiology-Lung Cellular and Molecular Physiology
910 297:L795–L802.

911 55. Moreau-Marquis S, Bomberger JM, Anderson GG, Swiatecka-Urban A, Ye S, O'Toole GA, Stanton
912 BA. 2008. The ΔF508-CFTR mutation results in increased biofilm formation by *Pseudomonas*
913 *aeruginosa* by increasing iron availability. American Journal of Physiology-Lung Cellular and
914 Molecular Physiology 295:L25–L37.

915 56. Bhowmik N, Stubbendieck RM. 2026. Natural products shape microbial ecology and disease in the
916 cystic fibrosis airway. Nat Prod Rep 10.1039.D6NP00067C.

917 57. Haas B, Kraut J, Marks J, Zanker SC, Castignetti D. 1991. Siderophore presence in sputa of cystic
918 fibrosis patients. Infect Immun 59:3997–4000.

919 58. Martin LW, Reid DW, Sharples KJ, Lamont IL. 2011. Pseudomonas siderophores in the sputum of
920 patients with cystic fibrosis. Biometals 24:1059–1067.

921 59. Takase H, Nitanai H, Hoshino K, Otani T. 2000. Impact of siderophore production on Pseudomonas
922 aeruginosa infections in immunosuppressed mice. Infect Immun 68:1834–1839.

bioRxiv preprint doi: https://doi.org/10.64898/2026.10.23.761465; this version posted October 31, 2026. The copyright holder for this preprint (which was not certified by peer review) is the author/funder, who has granted bioRxiv a license to display the preprint in perpetuity. It is made available under a CC-BY-NC-ND 4.0 International license.

923 60. Lehoux DE, Sanschagrin F, Levesque RC. 2000. Genomics of the 35-kb *pvd* locus and analysis of
924 novel *pvdIJK* genes implicated in pyoverdine biosynthesis in *Pseudomonas aeruginosa*. FEMS
925 Microbiology Letters 190:141–146.

926 61. Minandri F, Imperi F, Frangipani E, Bonchi C, Visaggio D, Facchini M, Pasquali P, Bragonzi A, Visca P.
927 2016. Role of Iron Uptake Systems in Pseudomonas aeruginosa Virulence and Airway Infection.
928 Infect Immun 84:2324–2335.

929 62. Nguyen AT, O'Neill MJ, Watts AM, Robson CL, Lamont IL, Wilks A, Oglesby-Sherrouse AG. 2014.
930 Adaptation of Iron Homeostasis Pathways by a Pseudomonas aeruginosa Pyoverdine Mutant in the
931 Cystic Fibrosis Lung. J Bacteriol 196:2265–2276.

932 63. Xiong YQ, Vasil ML, Johnson Z, Ochsner UA, Bayer AS. 2000. The oxygen- and iron-dependent sigma
933 factor pvdS of Pseudomonas aeruginosa is an important virulence factor in experimental infective
934 endocarditis. J Infect Dis 181:1020–1026.

935 64. Kirienko DR, Kang D, Kirienko NV. 2018. Novel Pyoverdine Inhibitors Mitigate Pseudomonas
936 aeruginosa Pathogenesis. Front Microbiol 9:3317.

937 65. Kang D, Kirienko NV. 2020. An In Vitro Cell Culture Model for Pyoverdine-Mediated Virulence.
938 Pathogens 10:9.

939 66. Meyer JM, Neely A, Stintzi A, Georges C, Holder IA. 1996. Pyoverdin is essential for virulence of
940 Pseudomonas aeruginosa. Infect Immun 64:518–523.

941 67. Kang D, Revtovich AV, Chen Q, Shah KN, Cannon CL, Kirienko NV. 2019. Pyoverdine-Dependent
942 Virulence of Pseudomonas aeruginosa Isolates From Cystic Fibrosis Patients. Front Microbiol
943 10:2048.

bioRxiv preprint doi: https://doi.org/10.64898/2026.10.23.761465; this version posted October 31, 2026. The copyright holder for this preprint (which was not certified by peer review) is the author/funder, who has granted bioRxiv a license to display the preprint in perpetuity. It is made available under a CC-BY-NC-ND 4.0 International license.

944 68. Reinhart A, Oglesby-Sherrouse A. 2016. Regulation of Pseudomonas aeruginosa Virulence by
945 Distinct Iron Sources. Genes 7:126.

946 69. Albrecht-Gary A-M, Blanc S, Rochel N, Ocaktan AZ, Abdallah MA. 1994. Bacterial Iron Transport:
947 Coordination Properties of Pyoverdin PaA, a Peptidic Siderophore of Pseudomonas aeruginosa.
948 Inorg Chem 33:6391–6402.

949 70. Brandel J, Humbert N, Elhabiri M, Schalk IJ, Mislin GLA, Albrecht-Gary A-M. 2012. Pyochelin, a
950 siderophore of Pseudomonas aeruginosa: Physicochemical characterization of the iron(iii),
951 copper(ii) and zinc(ii) complexes. Dalton Trans 41:2820.

952 71. Julou T, Mora T, Guillon L, Croquette V, Schalk IJ, Bensimon D, Desprat N. 2013. Cell–cell contacts
953 confine public goods diffusion inside *Pseudomonas aeruginosa* clonal microcolonies. Proc Natl
954 Acad Sci USA 110:12577–12582.

955 72. DePas WH, Starwalt-Lee R, Van Sambeek L, Ravindra Kumar S, Gradinaru V, Newman DK. 2016.
956 Exposing the Three-Dimensional Biogeography and Metabolic States of Pathogens in Cystic Fibrosis
957 Sputum via Hydrogel Embedding, Clearing, and rRNA Labeling. mBio 7:e00796-16.

958 73. Krüger A, Paik S-H, Bund M, Pesch M, Krueger S, Lückel B, Papadopoulos A, Wiechert J, Hassan T,
959 Weber U, Avellan R, Smits SHJ, Bott M, Kovács ÁT, Westhoff P, Matuszyńska A, Kohlheyer D, Drepper
960 T, Frunzke J. 2026. Context-dependent siderophore exploitability shapes microbial community
961 structure. The ISME Journal 20:wrag247.

962 74. Darling P, Chan M, Cox AD, Sokol PA. 1998. Siderophore Production by Cystic Fibrosis Isolates of
963 *Burkholderia cepacia*. Infect Immun 66:874–877.

bioRxiv preprint doi: https://doi.org/10.64898/2026.10.23.761465; this version posted October 31, 2026. The copyright holder for this preprint (which was not certified by peer review) is the author/funder, who has granted bioRxiv a license to display the preprint in perpetuity. It is made available under a CC-BY-NC-ND 4.0 International license.

964 75. Beasley FC, Vinés ED, Grigg JC, Zheng Q, Liu S, Lajoie GA, Murphy MEP, Heinrichs DE. 2009.
965 Characterization of staphyloferrin A biosynthetic and transport mutants in *Staphylococcus aureus*.
966 Molecular Microbiology 72:947–963.

967 76. Cotton JL, Tao J, Balibar CJ. 2009. Identification and Characterization of the *Staphylococcus aureus*
968 Gene Cluster Coding for Staphyloferrin A. Biochemistry 48:1025–1035.

969 77. García CA, Passerini De Rossi B, Alcaraz E, Vay C, Franco M. 2012. Siderophores of
970 Stenotrophomonas maltophilia: detection and determination of their chemical nature. Rev Argent
971 Microbiol 44:150–154.

972 78. Nas MY, Cianciotto NP. 2017. Stenotrophomonas maltophilia produces an EntC-dependent
973 catecholate siderophore that is distinct from enterobactin. Microbiology (Reading) 163:1590–1603.

974 79. Dashti Y, Nakou IT, Mullins AJ, Webster G, Jian X, Mahenthiralingam E, Challis GL. 2020. Discovery
975 and Biosynthesis of Bolagladins: Unusual Lipodepsipeptides from *Burkholderia gladioli* Clinical
976 Isolates**. Angew Chem Int Ed 59:21553–21561.

977 80. Dose B, Ross C, Niehs SP, Scherlach K, Bauer JP, Hertweck C. 2020. Food-Poisoning Bacteria Employ
978 a Citrate Synthase and a Type II NRPS To Synthesize Bolaamphiphilic Lipopeptide Antibiotics**.
979 Angew Chem Int Ed 59:21535–21540.

980 81. Witte Paz M, Bitzer A, Nieselt K, Heilbronner S. 2025. A landscape of metallophore synthesis and
981 uptake potential of the genus *Staphylococcus*. NAR Genomics and Bioinformatics 7:lqaf183.

982 82. Colautti J, Kelly SD, Whitney JC. 2025. Specialized killing across the domains of life by the type VI
983 secretion systems of Pseudomonas aeruginosa. Biochem J 482:1–15.

bioRxiv preprint doi: https://doi.org/10.64898/2026.10.23.761465; this version posted October 31, 2026. The copyright holder for this preprint (which was not certified by peer review) is the author/funder, who has granted bioRxiv a license to display the preprint in perpetuity. It is made available under a CC-BY-NC-ND 4.0 International license.

984 83. Elfarash A, Wei Q, Cornelis P. 2012. The soluble pyocins S2 and S4 from *P seudomonas aeruginosa*
985 bind to the same FpvAI receptor. MicrobiologyOpen 1:268–275.

986 84. Herzog E, Ishida K, Scherlach K, Chen X, Bartels B, Niehs SP, Cheaib B, Panagiotou G, Hertweck C.
987 2025. Antibacterial Siderophores of Pandoraea Pathogens and Their Impact on the Diseased Lung
988 Microbiota. Angew Chem Int Ed Engl 64:e202505714.

989 85. Turner KH, Wessel AK, Palmer GC, Murray JL, Whiteley M. 2015. Essential genome of *Pseudomonas*
990 *aeruginosa* in cystic fibrosis sputum. Proc Natl Acad Sci USA 112:4110–4115.

991 86. Dissanayake E, Brockman-Schneider RA, Stubbendieck RM, Helling BA, Zhang Z, Bochkov YA,
992 Kirkham C, Murphy TF, Ober C, Currie CR, Gern JE. 2023. Rhinovirus increases Moraxella catarrhalis
993 adhesion to the respiratory epithelium. Front Cell Infect Microbiol 12:1060748.

994 87. Wick RR, Howden BP, Stinear TP. 2025. Autocycler: long-read consensus assembly for bacterial
995 genomes. Bioinformatics 41:btaf474.

996 88. Kolmogorov M, Yuan J, Lin Y, Pevzner PA. 2019. Assembly of long, error-prone reads using repeat
997 graphs. Nat Biotechnol 37:540–546.

998 89. Cheng H, Concepcion GT, Feng X, Zhang H, Li H. 2021. Haplotype-resolved de novo assembly using
999 phased assembly graphs with hifiasm. Nat Methods 18:170–175.

1000 90. Chen S, Zhou Y, Chen Y, Gu J. 2018. Fastp: An ultra-fast all-in-one FASTQ preprocessor.
1001 Bioinformatics 34:i884–i890.

1002 91. Bankevich A, Nurk S, Antipov D, Gurevich AA, Dvorkin M, Kulikov AS, Lesin VM, Nikolenko SI, Pham
1003 S, Prjibelski AD, Pyshkin AV, Sirotkin AV, Vyahhi N, Tesler G, Alekseyev MA, Pevzner PA. 2012.

bioRxiv preprint doi: https://doi.org/10.64898/2026.10.23.761465; this version posted October 31, 2026. The copyright holder for this preprint (which was not certified by peer review) is the author/funder, who has granted bioRxiv a license to display the preprint in perpetuity. It is made available under a CC-BY-NC-ND 4.0 International license.

1004 SPAdes: a new genome assembly algorithm and its applications to single-cell sequencing. Journal of
1005 computational biology : a journal of computational molecular cell biology 19:455–77.

1006 92. Blin K, Shaw S, Vader L, Szenei J, Reitz ZL, Augustijn HE, Cediel-Becerra JDD, de Crécy-Lagard V,
1007 Koetsier RA, Williams SE, Cruz-Morales P, Wongwas S, Segurado Luchsinger AE, Biermann F,
1008 Korenskaia A, Zdouc MM, Meijer D, Terlouw BR, van der Hooft JJJ, Ziemert N, Helfrich EJN,
1009 Masschelein J, Corre C, Chevrette MG, van Wezel GP, Medema MH, Weber T. 2025. antiSMASH 8.0:
1010 extended gene cluster detection capabilities and analyses of chemistry, enzymology, and
1011 regulation. Nucleic Acids Res 53:W32–W38.

1012 93. Draisma A, Loureiro C, Louwen NLL, Kautsar SA, Navarro-Muñoz JC, Doering DT, Mouncey NJ,
1013 Medema MH. 2026. BiG-SCAPE 2.0 and BiG-SLiCE 2.0: scalable, accurate and interactive sequence
1014 clustering of metabolic gene clusters. Nat Commun 17:2000.

1015 94. Gu Z, Eils R, Schlesner M. 2016. Complex heatmaps reveal patterns and correlations in
1016 multidimensional genomic data. Bioinformatics (Oxford, England) 32:2847–9.

1017 95. Gilchrist CLM, Chooi Y-H. 2021. Clinker & clustermap.js: Automatic generation of gene cluster
1018 comparison figures. Bioinformatics (Oxford, England)
1019 https://doi.org/10.1093/bioinformatics/btab007.

1020 96. Hoang TT, Kutchma AJ, Becher A, Schweizer HP. 2000. Integration-Proficient Plasmids for
1021 Pseudomonas aeruginosa: Site-Specific Integration and Use for Engineering of Reporter and
1022 Expression Strains. Plasmid 43:59–72.

bioRxiv preprint doi: https://doi.org/10.64898/2026.10.23.761465; this version posted October 31, 2026. The copyright holder for this preprint (which was not certified by peer review) is the author/funder, who has granted bioRxiv a license to display the preprint in perpetuity. It is made available under a CC-BY-NC-ND 4.0 International license.

1023 97. Lusk HJ, Levy SE, Bergsten TM, Burdette JE, Sanchez LM. 2022. Home-Built Spinning Apparatus for
1024 Drying Agarose-Based Imaging Mass Spectrometry Samples. J Am Soc Mass Spectrom 33:1325–
1025 1328.

1026 98. Shepherd RA, Gad LY, Strobel M, Luu GT, Feng J, De Silva C, McKinnie SMK, Wang M, Sanchez LM.
1027 2026. MALDI Tandem Mass Spectrometry for Colony-Based Dereplication of Natural Products.
1028 bioRxiv 2026.06.21.733640.

1029 99. Chambers MC, Maclean B, Burke R, Amodei D, Ruderman DL, Neumann S, Gatto L, Fischer B, Pratt
1030 B, Egertson J, Hoff K, Kessner D, Tasman N, Shulman N, Frewen B, Baker TA, Brusniak M-Y, Paulse C,
1031 Creasy D, Flashner L, Kani K, Moulding C, Seymour SL, Nuwaysir LM, Lefebvre B, Kuhlmann F, Roark
1032 J, Rainer P, Detlev S, Hemenway T, Huhmer A, Langridge J, Connolly B, Chadick T, Holly K, Eckels J,
1033 Deutsch EW, Moritz RL, Katz JE, Agus DB, MacCoss M, Tabb DL, Mallick P. 2012. A cross-platform
1034 toolkit for mass spectrometry and proteomics. Nat Biotechnol 30:918–920.

1035 100. Wang M, Carver JJ, Phelan VV, Sanchez LM, Garg N, Peng Y, Nguyen DD, Watrous J, Kapono CA,
1036 Luzzatto-Knaan T, Porto C, Bouslimani A, Melnik AV, Meehan MJ, Liu W-T, Crüsemann M, Boudreau
1037 PD, Esquenazi E, Sandoval-Calderón M, Kersten RD, Pace LA, Quinn RA, Duncan KR, Hsu C-C, Floros
1038 DJ, Gavilan RG, Kleigrewe K, Northen T, Dutton RJ, Parrot D, Carlson EE, Aigle B, Michelsen CF,
1039 Jelsbak L, Sohlenkamp C, Pevzner P, Edlund A, McLean J, Piel J, Murphy BT, Gerwick L, Liaw C-C,
1040 Yang Y-L, Humpf H-U, Maansson M, Keyzers RA, Sims AC, Johnson AR, Sidebottom AM, Sedio BE,
1041 Klitgaard A, Larson CB, P CAB, Torres-Mendoza D, Gonzalez DJ, Silva DB, Marques LM, Demarque
1042 DP, Pociute E, O'Neill EC, Briand E, Helfrich EJN, Granatosky EA, Glukhov E, Ryffel F, Houson H,
1043 Mohimani H, Kharbush JJ, Zeng Y, Vorholt JA, Kurita KL, Charusanti P, McPhail KL, Nielsen KF, Vuong
1044 L, Elfeki M, Traxler MF, Engene N, Koyama N, Vining OB, Baric R, Silva RR, Mascuch SJ, Tomasi S,
1045 Jenkins S, Macherla V, Hoffman T, Agarwal V, Williams PG, Dai J, Neupane R, Gurr J, Rodríguez AMC,

bioRxiv preprint doi: https://doi.org/10.64898/2026.10.23.761465; this version posted October 31, 2026. The copyright holder for this preprint (which was not certified by peer review) is the author/funder, who has granted bioRxiv a license to display the preprint in perpetuity. It is made available under a CC-BY-NC-ND 4.0 International license.

Lamsa A, Zhang C, Dorrestein K, Duggan BM, Almaliti J, Allard P-M, Phapale P, Nothias L-F, Alexandrov T, Litaudon M, Wolfender J-L, Kyle JE, Metz TO, Peryea T, Nguyen D-T, VanLeer D, Shinn P, Jadhav A, Müller R, Waters KM, Shi W, Liu X, Zhang L, Knight R, Jensen PR, Palsson BO, Pogliano K, Linington RG, Gutiérrez M, Lopes NP, Gerwick WH, Moore BS, Dorrestein PC, Bandeira N. 2016. Sharing and community curation of mass spectrometry data with Global Natural Products Social Molecular Networking. Nature biotechnology 34:828–837.

101. Schmid R, Heuckeroth S, Korf A, Smirnov A, Myers O, Dyrlund TS, Bushuiev R, Murray KJ, Hoffmann N, Lu M, Sarvepalli A, Zhang Z, Fleischauer M, Dührkop K, Wesner M, Hoogstra SJ, Rudt E, Mokshyna O, Brungs C, Ponomarov K, Mutabdžija L, Damiani T, Pudney CJ, Earll M, Helmer PO, Fallon TR, Schulze T, Rivas-Ubach A, Bilbao A, Richter H, Nothias L-F, Wang M, Orešič M, Weng J-K, Böcker S, Jeibmann A, Hayen H, Karst U, Dorrestein PC, Petras D, Du X, Pluskal T. 2023. Integrative analysis of multimodal mass spectrometry data in MZmine 3. Nat Biotechnol 41:447–449.

102. Dührkop K, Fleischauer M, Ludwig M, Aksenov AA, Melnik AV, Meusel M, Dorrestein PC, Rousu J, Böcker S. 2019. SIRIUS 4: a rapid tool for turning tandem mass spectra into metabolite structure information. Nat Methods 16:299–302.

103. Bray NL, Pimentel H, Melsted PP, Pachter L. 2016. Near-optimal probabilistic RNA-seq quantification. Nature biotechnology 34:525–7.

104. Love MI, Huber W, Anders S. 2014. Moderated estimation of fold change and dispersion for RNA-seq data with DESeq2. Genome biology 15:550.

105. Zhu A, Ibrahim JG, Love MI. 2019. Heavy-tailed prior distributions for sequence count data: removing the noise and preserving large differences. Bioinformatics 35:2084–2092.

bioRxiv preprint doi: https://doi.org/10.64898/2026.10.23.761465; this version posted October 31, 2026. The copyright holder for this preprint (which was not certified by peer review) is the author/funder, who has granted bioRxiv a license to display the preprint in perpetuity. It is made available under a CC-BY-NC-ND 4.0 International license.

106. Bailey TL, Elkan C. 1994. Fitting a mixture model by expectation maximization to discover motifs in biopolymers. Proc Int Conf Intell Syst Mol Biol 2:28–36.

107. Stubbendieck RM, Dissanayake E, Burnham PM, Zelasko SE, Temkin MI, Wisdorf SS, Vrtis RF, Gern JE, Currie CR. 2023. Rothia from the Human Nose Inhibit Moraxella catarrhalis Colonization with a Secreted Peptidoglycan Endopeptidase. mBio e00464-23.

108. Cox J, Mann M. 2008. MaxQuant enables high peptide identification rates, individualized p.p.b.-range mass accuracies and proteome-wide protein quantification. Nat Biotechnol 26:1367–1372.

109. Winsor GL, Griffiths EJ, Lo R, Dhillon BK, Shay JA, Brinkman FSL. 2016. Enhanced annotations and features for comparing thousands of Pseudomonas genomes in the Pseudomonas genome database. Nucleic Acids Res 44:D646-653.

110. Wickham H. 2016. ggplot2: Elegant Graphics for Data Analysis. Springer-Verlag New York. http://ggplot2.org.

bioRxiv preprint doi: https://doi.org/10.64898/2026.10.23.761465; this version posted October 31, 2026. The copyright holder for this preprint (which was not certified by peer review) is the author/funder, who has granted bioRxiv a license to display the preprint in perpetuity. It is made available under a CC-BY-NC-ND 4.0 International license.

Tables

Table 1. *A. dolens* can induce pyoverdine production in clinical isolates of *Pseudomonas*.

Pyoverdine Production[1]		*pvdA* PCR Product[2]		
Monoculture (SCFM + 0 μM $FeCl_3$)	Coculture with *A. dolens* (SCFM + 25 μM $FeCl_3$)	Yes	No	Total
No	No	15	5	20
No	Yes	2	0	2
Yes	No	8	0	8
Yes	Yes	18	0	18
Total		43	5	48

[1]Pyoverdine production was scored by fluorescence after 24 h monoculture or coculture with *A. dolens* strain RMS0405. All isolates were screened in biological triplicate (independent experiments on different days). Nine isolates were inconsistent across the initial triplicates and the assays were repeated. On repeat, triplicates were consistent with each other and with the majority of replicates from the initial experiment.

[2]All isolates were screened by PCR using primers flanking *pvdA*. Isolates that were *pvdA*-negative were retested using genomic DNA extracted from a second culture to confirm absence of the PCR product.

bioRxiv preprint doi: https://doi.org/10.64898/2026.10.23.761465; this version posted October 31, 2026. The copyright holder for this preprint (which was not certified by peer review) is the author/funder, who has granted bioRxiv a license to display the preprint in perpetuity. It is made available under a CC-BY-NC-ND 4.0 International license.

Figure Legends

Figure 1. pwCF coinfected with *Achromobacter* and *Pseudomonas* exhibit more severe lung function outcomes. (**A**) Notched boxplot comparing lung function (FEV_1 pp) between pwCF without any detected pathogens (<1% relative abundance) and pwCF grouped based on pathogen presence (defined as ≥1% relative abundance). The upper and lower bounds of the notched box plots indicate the 75th and 25th percentiles, respectively. The horizontal black bars and notches represent the median and 95% confidence interval (CI) of the median, respectively. The whiskers extend from the bounds of the box to the largest and smallest values that are no further than 1.5× the IQR. Horizontal lines indicate pairwise comparisons against the both-pathogens group, with Benjamini-Hochberg (BH)-adjusted *P*-values from Wilcoxon rank-sum tests. (**B**) Proportion of pwCF in each group with severe disease (FEV_1 pp ≤ 30%). Points and lines show the proportion and 95% binomial CI. Horizontal lines indicate pairwise comparisons against the both-pathogens group, with BH-adjusted *P*-values from Fisher's exact test. (**C**) Association of coinfection of *Pseudomonas* and other CF pathogens on lung function after adjustment for age and BioProject. Samples missing either of these values were excluded. Points and error bars show the average change in adjusted lung function and 95% CI. Each estimate is the change relative to *Pseudomonas*-positive samples lacking the corresponding pathogen, with the other pathogens held constant. The dashed vertical line marks no difference. BH-corrected *P*-values from per-coefficient *t*-tests are indicated to the right of each comparison.

Figure 2. *A. dolens* induces pyoverdine production in *P. aeruginosa*. (**A**) Coculture of *A. dolens* RMS0405 (*Ad*, right) and *P. aeruginosa* strain PAO1 (left) on SCFM + 25 μM $FeCl_3$. Strains are labeled on the left: wild type (RMS0290), Δ*pvdA* (RMS0289), and Δ*pvdA* + *pvdA* (RMS0482). (**B**) Plate from panel **A** placed in a blue light transilluminator. Under blue light, pyoverdine exhibits fluorescence. (**C**) Cultures of *P.*

bioRxiv preprint doi: https://doi.org/10.64898/2026.10.23.761465; this version posted October 31, 2026. The copyright holder for this preprint (which was not certified by peer review) is the author/funder, who has granted bioRxiv a license to display the preprint in perpetuity. It is made available under a CC-BY-NC-ND 4.0 International license.

aeruginosa growing on SCFM + 25 µM $FeCl_3$ without *A. dolens* in a blue light transilluminator. All images are representative of triplicate samples. Scale bar is 5 mm.

Figure 3. *Achromobacter* spp. encode BGCs for alcaligin and other secondary metabolites. (**A**) Heat map of BGCs identified within *Achromobacter* spp. genomes (horizontal), organized based on a core genome phylogeny (top). Presence and absence of a BGC (rows) indicated in black and white, respectively. The alcaligin (*alc*) BGC is highlighted in gold. A putative NRP-metallophore BGC is highlighted in rust. The key for *Achromobacter* spp. isolation source, species, and pyoverdine (PVD) induction is indicated below. (**B**) Comparison of the *alc* BGC from *A. dolens* strain RMS0405 and *B. pertussis* strain Tohama I. Darker shading corresponds to higher sequence identity, as indicated by the scale below. Gene color corresponds to protein function, as indicated by the key below. Scale bar is 1.0 kb. See **Fig. S2** in the supplemental material for comparisons to the corresponding BGCs from all *Achromobacter* spp. (**C**) Structure, formula, and predicted molecular mass of alcaligin. (**D**) CAS assay results from (i) a negative control, (ii) an ethylenediaminetetraacetic acid (EDTA) positive control, (iii) culture extract from *A. dolens* strain RMS0405. (iv) The culture extract without addition of CAS reagent.

Figure 4. Production of Siderophores during coculture of *A. dolens* and *P. aeruginosa*. Mass spectrometry imaging of coculture of *A. dolens* strain RMS0405 (*Ad*, right) and *P. aeruginosa* strain PAO1 on SCFM + 25 μM $FeCl_3$. (**A-B**) False-colored blue light image of *P. aeruginosa* (**A**) wild type and (**B**) Δ*pvdA* and *A. dolens*. (**C-D**) Extracted ion images of molecular features ($[M+H]^+$) for pyoverdine in *P. aeruginosa* (**C**) wild type and (**D**) Δ*pvdA*. (**E-F**) Extracted ion images of $[M+H]^+$ for alcaligin in coculture between *P. aeruginosa* (**E**) wild type and (**F**) Δ*pvdA* and *A. dolens*. (**G-H**) Extracted ion images of $[M+H]^+$ for pyochelin in coculture between *P. aeruginosa* (**G**) wild type and (**H**) Δ*pvdA* and *A. dolens*. Brighter pixels indicate higher signal of the corresponding $[M+H]^+$. Note, the ion intensity for a given molecular feature is

bioRxiv preprint doi: https://doi.org/10.64898/2026.10.23.761465; this version posted October 31, 2026. The copyright holder for this preprint (which was not certified by peer review) is the author/funder, who has granted bioRxiv a license to display the preprint in perpetuity. It is made available under a CC-BY-NC-ND 4.0 International license.

comparable between the cocultures with *P. aeruginosa* wild type (left images) and Δ*pvdA* (right images), but not between different ions due to differences in ionization efficiency. All *m/z* values are ± 4.6 parts per million (ppm). Scale bar is 5 mm. Experiment is representative of duplicate samples. See **Figs. S4** and **S5** in the supplemental material for extracted ion images of potential alcaligin analogues and known *P. aeruginosa* secondary metabolites, respectively.

Figure 5. Iron modulates pyoverdine induction during *A. dolens*-*P. aeruginosa* cocultures. (**A-C**) Coculture of *A. dolens* strain RMS0405 (*Ad*, right) and *P. aeruginosa* strain PAO1 (left) on SCFM with (**A**) no supplemented $FeCl_3$ (+ 0 μM), (**B**) supplemented with 25 μM $FeCl_3$ (+ 25 μM), and (**C**) supplemented with 100 μM $FeCl_3$ (+ 100 μM). (**D-F**) Monoculture controls of *P. aeruginosa* on SCFM with (**D**) no supplemented $FeCl_3$ (+ 0 μM), (**E**) supplemented with 25 μM $FeCl_3$ (+ 25 μM), and (**F**) supplemented with 100 μM $FeCl_3$ (+ 100 μM). Strains are labeled on the left: wild type (RMS290), Δ*pvdA* (RMS0289), and Δ*pvdA* + *pvdA* (RMS0482). All images are representative of duplicate samples taken under a blue light transilluminator. Scale bar is 5 mm.

Figure 6. Coculture with *A. dolens* induces a low-iron stress response in *P. aeruginosa*. (**A**) Volcano plot showing the fold change of genes from *P. aeruginosa* strain PAO1 that were detected in SCFM supplemented with 25 μM $FeCl_3$ either in monoculture or coculture with *A. dolens* strain RMS0405. Each point represents a gene, and its size corresponds to the normalized read count, as indicated below. The color of the points indicates protein functional category, as indicated below. The horizontal dashed line indicates the BH-adjusted *P*-value threshold of 0.05 for significance. The genes involved in pyoverdine biosynthesis and exotoxin production and regulated are highlighted. (**B**) Sequence logo for 105 predicted FBS sequences in the *P. aeruginosa* strain PAO1 genome. (**C**) Subset of the volcano plot in **A** only showing genes with a predicted FBS. Inset: box plots of the percentage of *P. aeruginosa* strain PAO1 genes with

bioRxiv preprint doi: https://doi.org/10.64898/2026.10.23.761465; this version posted October 31, 2026. The copyright holder for this preprint (which was not certified by peer review) is the author/funder, who has granted bioRxiv a license to display the preprint in perpetuity. It is made available under a CC-BY-NC-ND 4.0 International license.

putative FBS with increased expression in monoculture (blue), with increased expression in coculture with *A. dolens* strain RMS0405 (red), or were not differentially regulated (grey). Each box summarizes eight results obtained by withholding one sample and repeating the differential expression analysis. The upper and lower bounds of the box plots indicate the 75th and 25th percentiles, respectively. The horizontal black bar indicates the median. Conditions that share a letter are not significantly different (BH-adjusted $P > 0.05$). (**D**) Plot showing *P. aeruginosa* strain PAO1 pathways increased or decreased during coculture with *A. dolens* strain RMS0405. The color and size of each point represents the $-\log_{10}$ BH-adjusted *P* value and the fraction of genes differentially regulated, respectively, as indicated below.

Figure 7. Coculture with *A. dolens* stimulates virulence factor production by *P. aeruginosa*. Volcano plot showing the fold change of proteins from *P. aeruginosa* strain PAO1 that were detected in SCFM supplemented with 25 μM $FeCl_3$ either in monoculture or coculture with *A. dolens* strain RMS0405. Each point represents a protein, and its size corresponds to the normalized protein intensity, as indicated below. The color of the points indicates protein functional category, as indicated below. The horizontal and vertical dashed lines indicates the BH-adjusted *P*-value and $\log_2$ fold change thresholds for significance. Specific virulence factors, the hemophore HasAp, and pyocin S4 are highlighted.

bioRxiv preprint doi: https://doi.org/10.64898/2026.10.23.761465; this version posted October 31, 2026. The copyright holder for this preprint (which was not certified by peer review) is the author/funder, who has granted bioRxiv a license to display the preprint in perpetuity. It is made available under a CC-BY-NC-ND 4.0 International license.

Supplemental Material

Figure S1. The severity of *Achromobacter-Pseudomonas* coinfections increases with pathogen relative abundance. (**A**) Effect of coinfection of *Pseudomonas* and *Achromobacter* on FEV_1 pp after adjustment for age and BioProject, repeated across different relative abundance thresholds. Samples missing either of these values were excluded. Points and error bars show the average change in adjusted FEV_1 pp and 95% CI. Each estimate is the change relative to *Pseudomonas*-positive samples lacking *Achromobacter*, with the other pathogens held constant. The dashed vertical line marks no difference. BH-corrected *P*-values from per-coefficient *t*-tests are indicated to the right of each comparison. (**B**) Among pwCF coinfected with *Achromobacter* and *Pseudomonas*, lung function versus combined relative abundance of *Achromobacter* or *Pseudomonas*. The pies represent the relative abundance of *Achromobacter* (dark-red), *Pseudomonas* (yellow-green), and other bacteria (gray). Pies are jittered to avoid overplotting. The dashed vertical line separates samples that are pathogen-dominated on the right from those that are not on the left. The line is the ordinary least squares fit with its 95% confidence band. Spearman's ρ and *P*-value are indicated at top-right.

Figure S2. The *alc* BGC of *Achromobacter* spp. are highly conserved. Comparison of *alc* BGCs from *Achromobacter* spp. and *B. pertussis* strain Tohama I (BGC0002464). Darker shading corresponds to higher sequence identity, as indicated by the scale below. Each color corresponds to a distinct homologue. The genes in the *alc* BGC are labeled. Scale bar is 1.0 kb.

Figure S3. Alcaligin biosynthesis genes are conserved in *Achromobacter* spp. (**A**) Biosynthetic pathway for alcaligin from L-ornithine. (**B**) Heatmap showing sequence identity of genes required to synthesize alcaligin across *Achromobacter* spp. compared to *B. pertussis* strain Tohama I. A gene was considered

bioRxiv preprint doi: https://doi.org/10.64898/2026.10.23.761465; this version posted October 31, 2026. The copyright holder for this preprint (which was not certified by peer review) is the author/funder, who has granted bioRxiv a license to display the preprint in perpetuity. It is made available under a CC-BY-NC-ND 4.0 International license.

present when its best hit spanned at least 70% of the reference length at ≥30% identity, and genes failing these thresholds are drawn as white tiles marked with an X.

Figure S4. Mass spectrometry imaging of alcaligin analogues produced during coculture of *A. dolens* and *P. aeruginosa*. Mass spectrometry imaging of coculture of *A. dolens* strain RMS0405 (*Ad*, right) and *P. aeruginosa* strain PAO1 on SCFM + 25 μM $FeCl_3$. (**A-B**) False-colored blue light image of *P. aeruginosa* (**A**) wild type and (**B**) Δ*pvdA* and *A. dolens*. (**C-D**) Extracted ion images of $[M+H]^+$ for alcaligin in coculture between *P. aeruginosa* (**C**) wild type and (**D**) Δ*pvdA* and *A. dolens*. (**E-F**) Extracted ion images of $[M+H]^+$ for molecule that may be alcaligin in coculture between *P. aeruginosa* (**E**) wild type and (**F**) Δ*pvdA* and *A. dolens*. (**G-H**) Extracted ion images of $[M+H]^+$ for molecule that may be an alcaligin analogue in coculture between *P. aeruginosa* (**G**) wild type and (**H**) Δ*pvdA* and *A. dolens*. Note, the ion intensity for a given molecular feature is comparable between the cocultures with *P. aeruginosa* wild type (left images) and Δ*pvdA* (right images), but not between different ions due to differences in ionization efficiency. All *m/z* values are ± 4.6 parts per million (ppm). Scale bar is 5 mm. Experiment is representative of duplicate samples.

Figure S5. Double pyochelin and pyoverdine biosynthesis mutant exhibits a minor growth defect with cultured with *A. dolens* strain RMS0405. (**A**) Coculture of *A. dolens* strain RMS0405 (right) and *P. aeruginosa* strain PAO1 (left) on SCFM with no supplemented $FeCl_3$. (**B**) Plate from panel **A** placed in a blue light transilluminator. (**C**) Cultures of *P. aeruginosa* growing on SCFM with no supplemented $FeCl_3$. (**D**) Plate from panel **C** placed in a blue light transilluminator. Strains are labeled on the left: wild type (RMS290), Δ*pvdA* (RMS0289), Δ*pchA* (RMS0494), and Δ*pvdA* Δ*pchA* (RMS0489). All images are representative of duplicate samples taken under a blue light transilluminator. Scale bar is 5 mm.

bioRxiv preprint doi: https://doi.org/10.64898/2026.10.23.761465; this version posted October 31, 2026. The copyright holder for this preprint (which was not certified by peer review) is the author/funder, who has granted bioRxiv a license to display the preprint in perpetuity. It is made available under a CC-BY-NC-ND 4.0 International license.

Figure S6. Mass spectrometry imaging of known *P. aeruginosa* secondary metabolites produced during coculture with *A. dolens*. Mass spectrometry imaging of coculture of *A. dolens* strain RMS0405 (Ad, right) and *P. aeruginosa* strain PAO1 on SCFM + 25 μM $FeCl_3$. **(A-B)** False-colored blue light image of *P. aeruginosa* **(A)** wild type and **(B)** Δ*pvdA* and *A. dolens*. **(C-D)** Extracted ion images of molecular features ($[M+H]^+$) for pyoverdine in *P. aeruginosa* **(C)** wild type and **(D)** Δ*pvdA*. **(E-F)** Extracted ion images of $[M+H]^+$ for pyochelin in coculture between *P. aeruginosa* **(E)** wild type and **(F)** Δ*pvdA* and *A. dolens*. **(G-H)** Extracted ion images of $[M+H]^+$ for pyocyanin in coculture between *P. aeruginosa* **(G)** wild type **(H)** and Δ*pvdA* and *A. dolens*. **(I-J)** Extracted ion images of $[M+H]^+$ for phenazine-1-carboxylic acid in coculture between *P. aeruginosa* **(I)** wild type and **(J)** Δ*pvdA* and *A. dolens*. **(K-L)** Extracted ion images of $[M+H]^+$ for phenazine dicarboxylic acid in coculture between *P. aeruginosa* **(K)** wild type and **(L)** Δ*pvdA* and *A. dolens*. **(M-N)** Extracted ion images of $[M+H]^+$ for phenazine-1-carboxamide in coculture between *P. aeruginosa* **(M)** wild type and **(N)** Δ*pvdA* and *A. dolens*. **(O-P)** Extracted ion images of $[M+H]^+$ for Pseudomonas quinolone signal in coculture between *P. aeruginosa* **(O)** wild type and **(P)** Δ*pvdA* and *A. dolens*. **(Q-R)** Extracted ion images of $[M+H]^+$ for 2-heptyl-4-quinolone in coculture between *P. aeruginosa* **(Q)** wild type and **(R)** Δ*pvdA* and *A. dolens*. **(S-T)** Extracted ion images of $[M+H]^+$ for Rha-Rha-C10-C10 in coculture between *P. aeruginosa* **(S)** wild type and **(T)** Δ*pvdA* and *A. dolens*. Brighter pixels indicate higher signal of the corresponding $[M+H]^+$. Note, the ion intensity for a given molecular feature is comparable between the cocultures with *P. aeruginosa* wild type (left images) and Δ*pvdA* (right images), but not between different ions due to differences in ionization efficiency. All m/z values are ± 4.6 parts per million (ppm). Scale bar is 5 mm. Experiment is representative of duplicate samples.

bioRxiv preprint doi: https://doi.org/10.64898/2026.10.23.761465; this version posted October 31, 2026. The copyright holder for this preprint (which was not certified by peer review) is the author/funder, who has granted bioRxiv a license to display the preprint in perpetuity. It is made available under a CC-BY-NC-ND 4.0 International license.

Figure S7. Assignment of molecular features produced by *A. dolens* strain RMS0405 and *P. aeruginosa* strain PAO1 as siderophores. Evidence for the assignment of (**A**) *m/z* 1333.6177 as pyoverdine E, (**B**) *m/z* 405.1866 as alcaligin, and (**C**) *m/z* 325.0692 as pyochelin.

Table S1. Accessions and metadata for amplicon sequencing samples analyzed in this study.

Table S2. Individual growth and pyoverdine production results from cocultures between *A. dolens* and 48 clinical *Pseudomonas* isolates used in this study.

Table S3. Expression data for all genes in *P. aeruginosa* strain PAO1 in monoculture and during coculture with *A. dolens* strain RMS0405.

Table S4. Predicted genes in *P. aeruginosa* strain PAO1 with FBS-containing promoters.

Table S5. Differentially expressed genes in *P. aeruginosa* strain PAO1 related to iron in monoculture and during coculture with *A. dolens* strain RMS0405.

Table S6. Proteins detected in *P. aeruginosa* strain PAO1 during monoculture and during coculture with *A. dolens* strain RMS0405. The localization of each protein is indicated in the table.

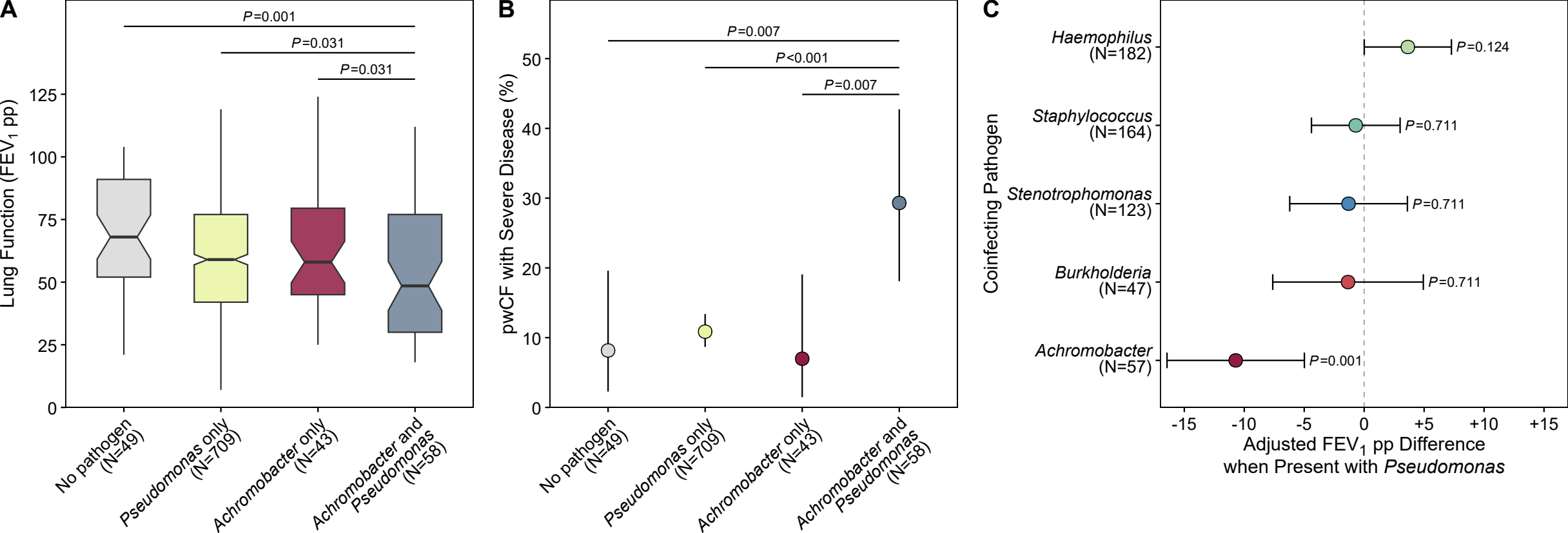
Table S7. Metadata for *Achromobacter* spp. used in this study. Genomic sequencing statistics are provided for strains sequenced as part of this study.

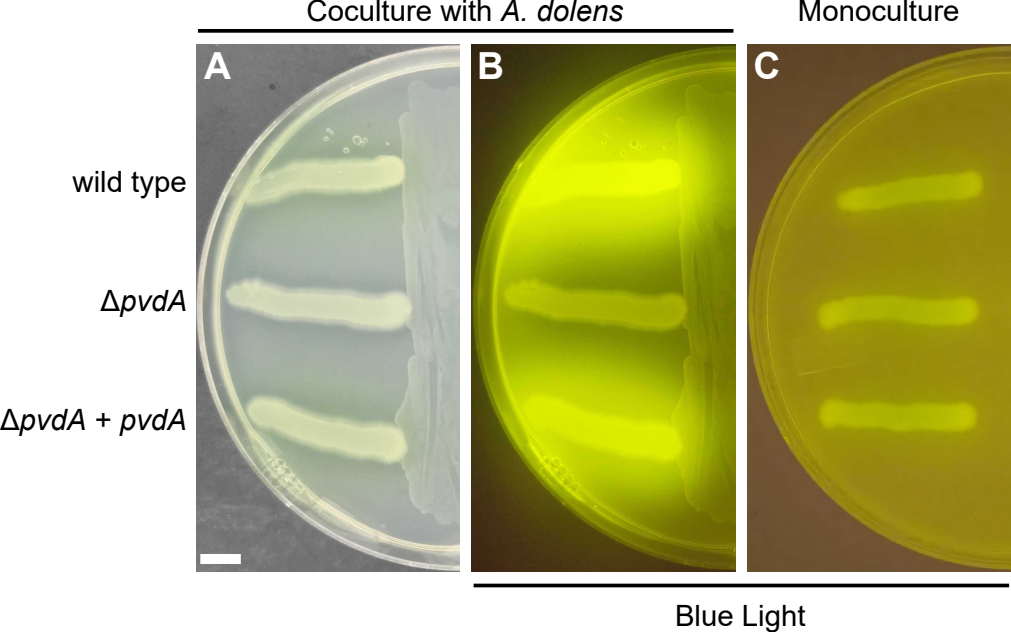
Table S8. MALDI-TOF-MSI method parameters for acquisition.

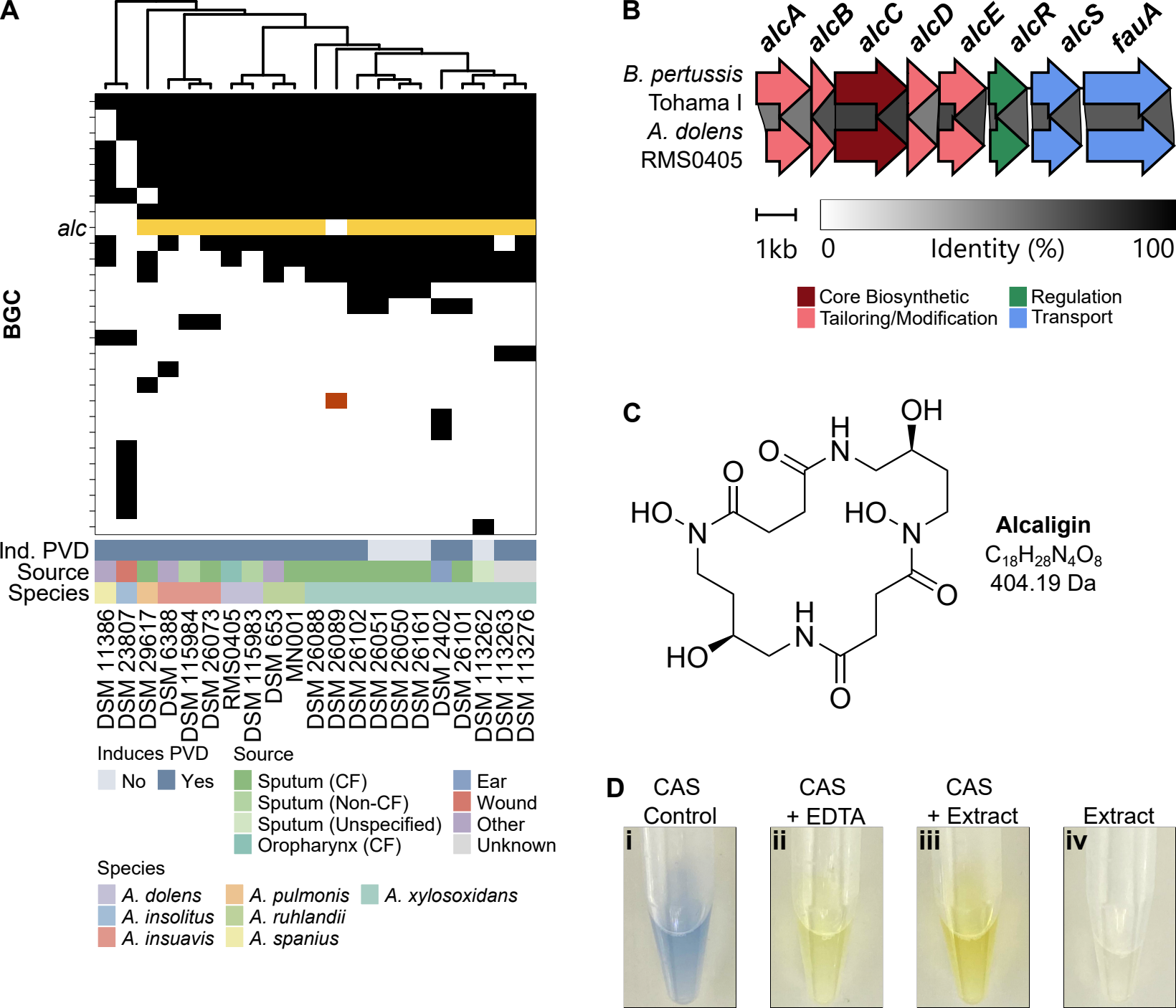
bioRxiv preprint doi: https://doi.org/10.64898/2026.10.23.761465; this version posted October 31, 2026. The copyright holder for this preprint (which was not certified by peer review) is the author/funder, who has granted bioRxiv a license to display the preprint in perpetuity. It is made available under a CC-BY-NC-ND 4.0 International license.

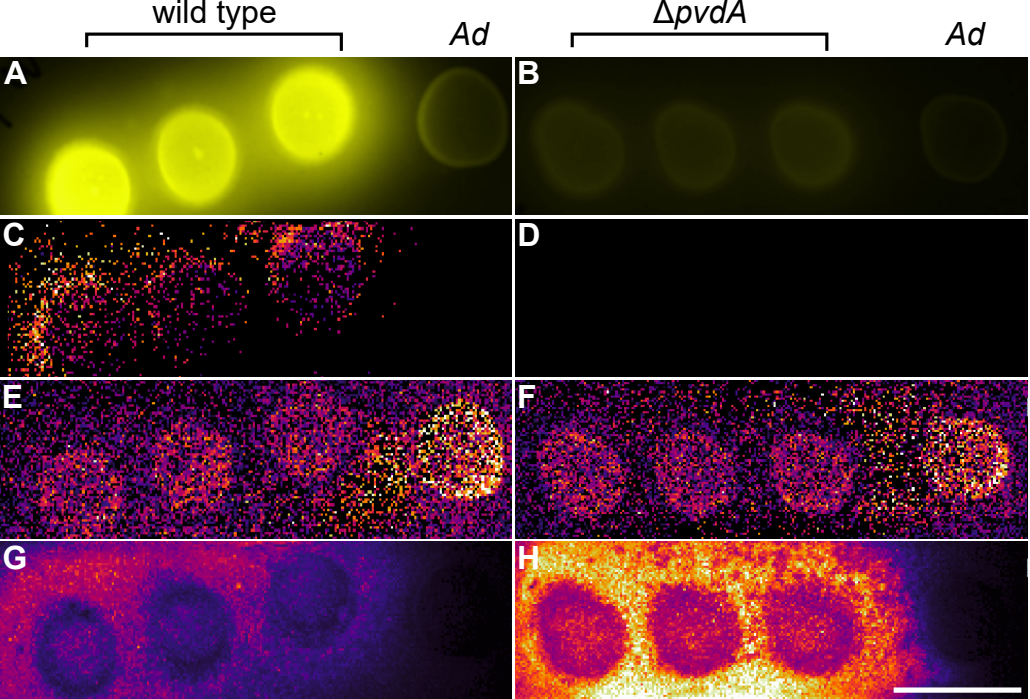
1275

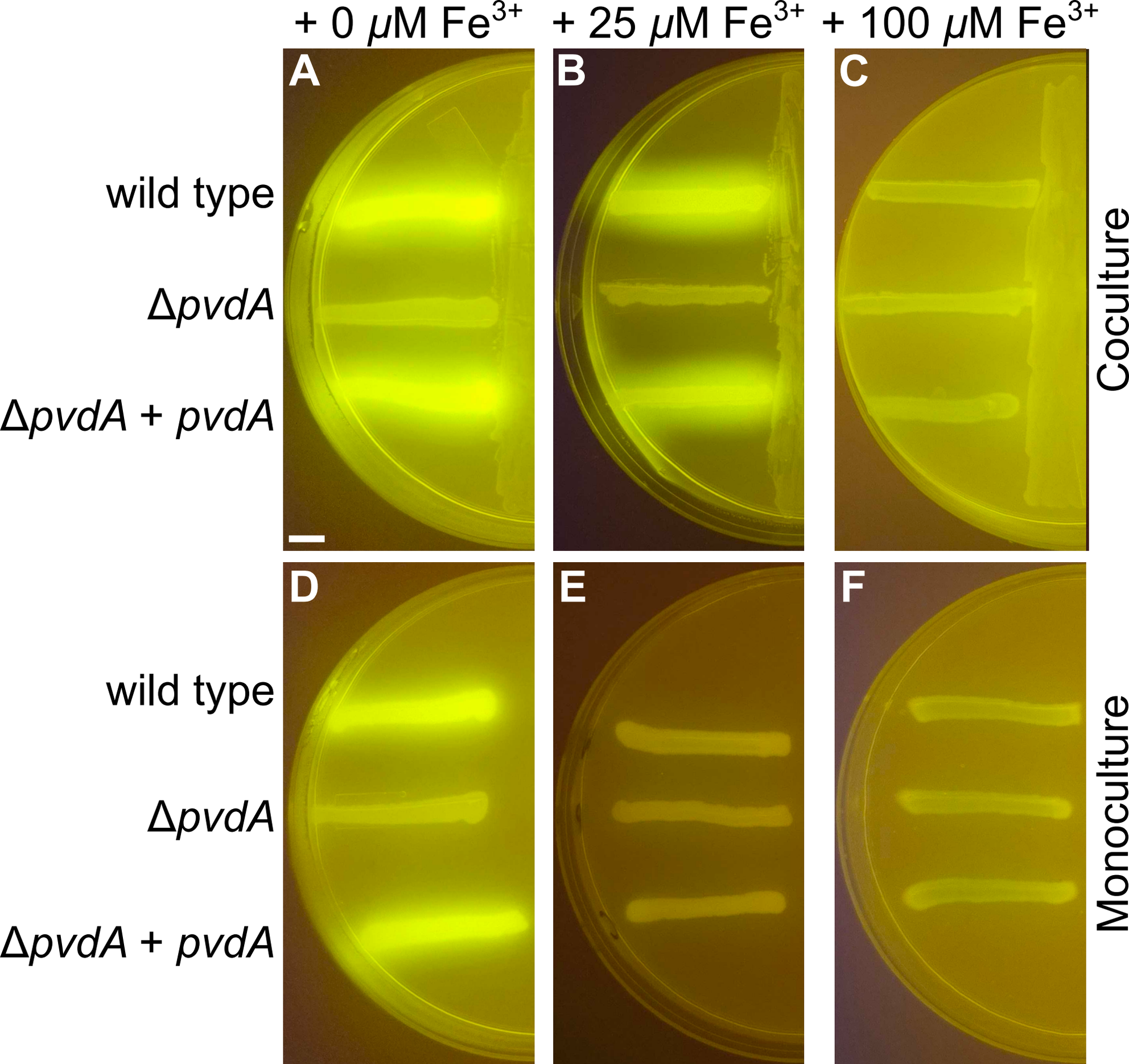
1276 **Table S9**. MALDI-DDA-MS method parameters for acquisition.

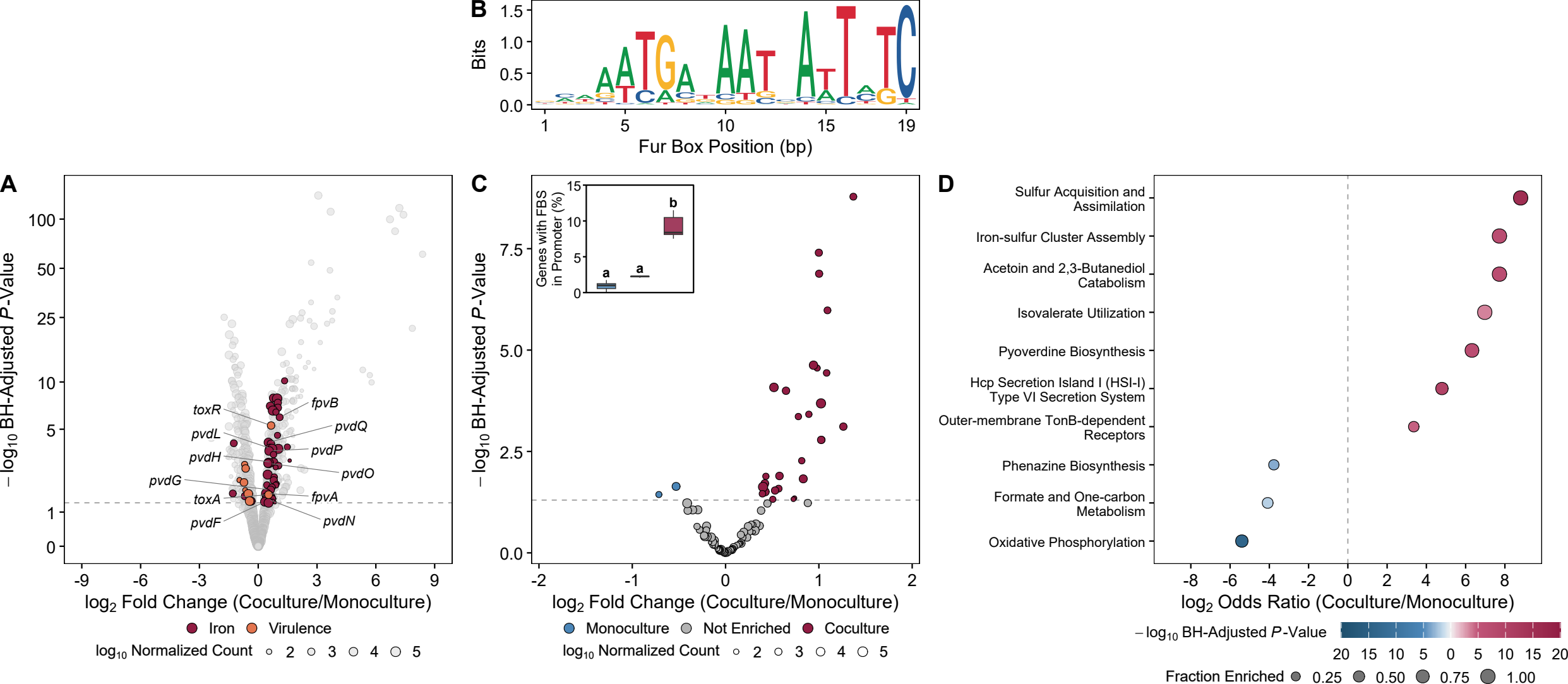

A
P=0.001
P=0.031
P=0.031
Lung Function (FEV1 pp)
125
100
75
50
25
0
No pathogen (N=49)
Pseudomonas only (N=709)
Achromobacter only (N=43)
Achromobacter and Pseudomonas (N=58)
B
P=0.007
P<0.001
P=0.007
pwCF with Severe Disease (%)
50
40
30
20
10
0
No pathogen (N=49)
Pseudomonas only (N=709)
Achromobacter only (N=43)
Achromobacter and Pseudomonas (N=58)
C
Coinfecting Pathogen
Haemophilus (N=182)
P=0.124
Staphylococcus (N=164)
P=0.711
Stenotrophomonas (N=123)
P=0.711
Burkholderia (N=47)
P=0.711
Achromobacter (N=57)
P=0.001
-15
-10
-5
0
+5
+10
+15
Adjusted FEV1 pp Difference when Present with Pseudomonas

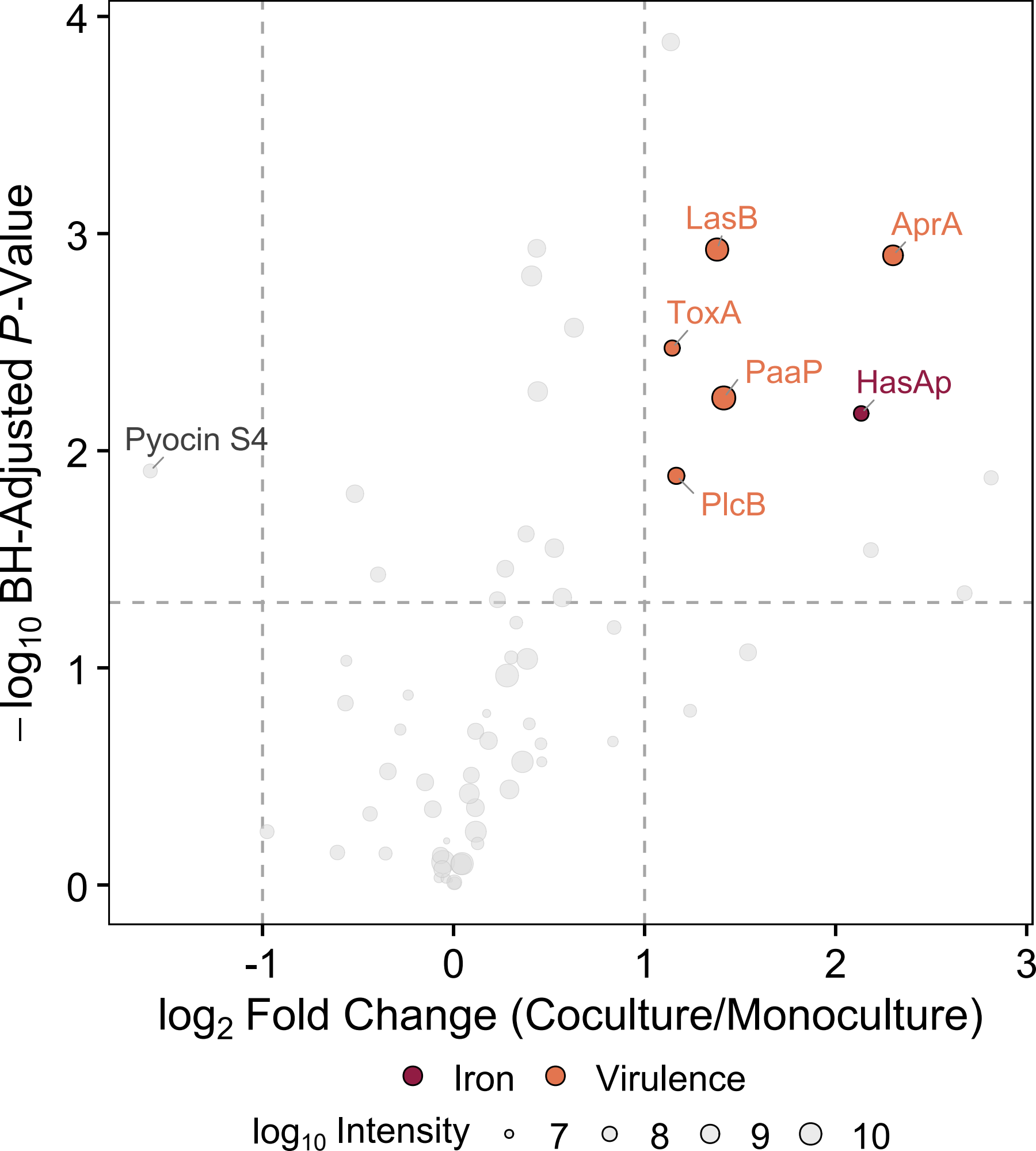

Coculture with A. dolens
Monoculture
A
B
C
wild type
ΔpvdA
ΔpvdA + pvdA
Blue Light


A
alc
BGC
Ind. PVD
Source
Species
DSM 11386
DSM 23807
DSM 29617
DSM 6388
DSM 115984
DSM 26073
RMS0405
DSM 115983
DSM 653
MN001
DSM 26088
DSM 26089
DSM 26102
DSM 26051
DSM 26050
DSM 26161
DSM 2402
DSM 26101
DSM 113262
DSM 113263
DSM 113276
Induces PVD
No
Yes
Source
Sputum (CF)
Sputum (Non-CF)
Sputum (Unspecified)
Oropharynx (CF)
Ear
Wound
Other
Unknown
Species
A. dolens
A. insolitus
A. insuavis
A. pulmonis
A. ruhlandii
A. spanius
A. xylosoxidans
B
alcA
alcB
alcC
alcD
alcE
alcR
alcS
fauA
B. pertussis Tohama I
A. dolens RMS0405
1kb
0
Identity (%)
100
Core Biosynthetic
Tailoring/Modification
Regulation
Transport
C
HO
N
O
H
N
OH
HO
N
O
HO
H
N
O
Alcaligin
C18H28N4O8
404.19 Da
D
CAS Control
CAS + EDTA
CAS + Extract
Extract
i
ii
iii
iv


wild type
Ad
ΔpvdA
Ad
A
B
Blue Light
C
D
m/z 1333.6177
Pyoverdine
E
F
m/z 405.1866
Alcaligin
G
H
m/z 325.0692
Pyochelin


+ 0 μM Fe3+
+ 25 μM Fe3+
+ 100 μM Fe3+
A
B
C
D
E
F
wild type
ΔpvdA
ΔpvdA + pvdA
wild type
ΔpvdA
ΔpvdA + pvdA
Coculture
Monoculture


B
Bits
1.5
1.0
0.5
0.0
1
5
10
15
19
Fur Box Position (bp)
A
$-\log_{10}$ BH-Adjusted P-Value
100
50
25
10
5
1
0
toxR
pvdL
pvdH
pvdG
toxA
pvdF
fpvB
pvdQ
pvdP
pvdO
fpvA
pvdN
-9
-6
-3
0
3
6
9
$\log_2$ Fold Change (Coculture/Monoculture)
Iron
Virulence
$\log_{10}$ Normalized Count
2
3
4
5
C
$-\log_{10}$ BH-Adjusted P-Value
7.5
5.0
2.5
0.0
Genes with FBS in Promoter (%)
15
10
5
0
a
a
b
-2
-1
0
1
2
$\log_2$ Fold Change (Coculture/Monoculture)
Monoculture
Not Enriched
Coculture
$\log_{10}$ Normalized Count
2
3
4
5
D
Sulfur Acquisition and Assimilation
Iron-sulfur Cluster Assembly
Acetoin and 2,3-Butanediol Catabolism
Isovalerate Utilization
Pyoverdine Biosynthesis
Hcp Secretion Island I (HSI-I) Type VI Secretion System
Outer-membrane TonB-dependent Receptors
Phenazine Biosynthesis
Formate and One-carbon Metabolism
Oxidative Phosphorylation
-8
-6
-4
-2
0
2
4
6
8
$\log_2$ Odds Ratio (Coculture/Monoculture)
$-\log_{10}$ BH-Adjusted P-Value
20
15
10
5
0
5
10
15
20
Fraction Enriched
0.25
0.50
0.75
1.00


LasB
AprA
ToxA
PaaP
HasAp
Pyocin S4
PlcB
4
3
2
1
0
-1
0
1
2
3
− log10 BH-Adjusted P-Value
log2 Fold Change (Coculture/Monoculture)
Iron
Virulence
log10 Intensity
7
8
9
10